EGG-SSRE--7906

DE88 006787

DISCLAIMER

EXTENSION AND ASSESSMENT OF THE CLADDING BALLOONING MODEL IN THE FRAP-T6 CODE

Karim El-Adham*

Published May 1987

EG&G Idaho, Inc.
Idaho Falls, Idaho 83415

Prepared in part for the
U.S. Department of Energy
Idaho Operations Office
Under DOE Contract No. DE-AC07-76ID01570

*Training at EG&G, Idaho under an International Atomic Energy Agency Fellowship Program.

ABSTRACT

The FRAP-T6 code was extended to calculate: (a) fuel surface azimuthal temperature distribution; (b) work done on cladding by internal pressure; and (c) azimuthal heat conduction in the cladding. The extensions were assessed by comparing calculated and measured cladding ballooning characteristics for four in-pile fuel rod tests. The assessment showed that the calculation of the fuel surface azimuthal temperature distribution improved the calculations of cladding ballooning. Both calculations and experimental results indicate that coplanar blockage due to cladding ballooning is unlikely during a large break LOCA.

CONTENTS

FIGURES

TABLES

EXTENSION AND ASSESSMENT OF THE CLADDING BALLOONING MODEL IN THE FRAP-T6 CODE

1. INTRODUCTION

The effect of cladding ballooning and rupture on cooling of the reactor core during a postulated loss-of-coolant accident has been identified as a safety issue for pressurized water reactors.[1] In particular, the point of debate is whether or not cladding ballooning and rupture can lead to coplanar blockage and loss of coolable geometry. If certain conditions are met, experimental results show that a large amount of ballooning is possible. For example, circumferential strains have exceeded 70% during alpha phase ballooning of irradiated test fuel rods in PBF single rod tests,[2] while similar ballooning of single simulator fuel rods in heated shrouds at low heating rates have resulted in circumferential strains of over 100%.[3] Circumferential cladding strains of 65% may cause complete flow blockage in a PWR rod bundle.

The understanding of the phenomena involved in cladding ballooning is vital in a calculation of the extent of coolant channel blockage caused by ballooning. Fuel rod ballooning and rupture behavior is primarily dependent on: (a) cladding temperature distribution; (b) cladding heating rate; and (c) amount of cladding oxidation. The effect of these variables on cladding ballooning is calculated by Hagrman's model for ballooning.[4] This model, named BALON2, is a best-estimate mechanistic model that considers all of the important phenomena taking place during ballooning. This code is a part of the FRAP-T6 code,[5] which predicts the transient response of a light water reactor fuel rod during hypothetical accidents.

The BALON2 code computes the extent and shape of the cladding deformation. The cladding is modeled as a network of membrane elements subjected to a pressure difference across the wall. The equations for the model in the code are derived from the equation of equilibrium and geometric constraints. Sdouz has extended BALON2 to a fuel behavior code

named BALO-2A.[6] This code covers most of the thermomechanical effects but does not include fission gas behavior. Sdouz extended BALON2 to include azimuthal conduction in the cladding.

This report documents two further extensions to the BALON2 code and the assessment of the extended code. The first extension consisted of adding a model to calculate the azimuthal heat conduction in the fuel as well as the cladding. This model is important because the cladding azimuthal temperature distribution is a function of the fuel surface temperature distribution. The second extension consisted of adding a term in the cladding heat conduction equation that accounts for the heat generated in the cladding due to the work done by the stress across a circumferential strain. These extensions of the BALON2 code are described in Section 2 of this report. Section 3 describes the in-pile ballooning tests that were used to assess the extended BALON2 code. An assessment of the extended BALON2 code based on comparison of calculations and test measurements is presented in Section 4. An in-depth study of the model extensions is given in Section 5. Conclusions are presented in Section 6.

2. DESCRIPTION OF MODIFICATIONS TO BALLOONING MODEL

The modifications focused on three areas: (a) calculation of the fuel surface azimuthal temperature distribution; (b) calculation of the work done on the cladding by internal pressure; and (c) the modeling of azimuthal heat conduction in the cladding.

The method developed by Nijsing[8] for nonconcentric fuel and cladding was used for the determination of the fuel surface azimuthal temperature distribution. The infinite series solution that his method employs was truncated after four terms. The boundary conditions were imposed at five azimuthal locations between azimuthal coordinates of zero to 2 π, which results in a set of five linear equations with five unknowns. The five values of the five unknowns were solved by Gaussian elimination. The resulting equation for fuel surface temperature distribution was used in place of the original BALON2 assumption of a 100 K difference between minimum and maximum fuel surface temperature.

The rate of heat generation by the work of internal pressure on the cladding was calculated by the equation:

$$\dot{W} = 2\pi \text{ (circumferential stress)(circumferential strain rate)(average cladding radius)(initial cladding thickness)exp(radial strain)}$$

where

stress is in units of N/m^2, strain rate in units of s^{-1}, and radius and thickness in units of m.

The heat conduction in the azimuthal direction in the cladding was solved by using an explicit finite difference equation.

3. DESCRIPTION OF TESTS USED FOR ASSESSING THE BALLOONING MODEL

A total of four in-pile experiments on fuel rod ballooning were used to assess the extensions made to the ballooning model in FRAP-T6. Each of these experiments was performed in a different reactor. The four experiments were: (a) PBF LOC-3 experiment in the USA;[9] (b) KfK FR2 LOCA experiment in the FRG;[10] (c) International Standard Problem 19 LOCA experiment in France;[11] and (d) TREAT FRF-2 experiment in the USA.[12]

3.1 PBF LOCA Test (LOC-3)

The PBF LOC-3 test was carried out in the Power Burst Facility (PBF) at the Idaho National Engineering Laboratory. The test aimed to: (a) determine the effects of the internal fuel rod pressure and prior irradiation on the deformation behavior of fuel rods that reach cladding peak temperatures in the α-β phase of zircaloy; (b) evaluate the possibility of coplanar blockage and subsequent loss of coolable geometry that may result from cladding ballooning during a LOCA; and (c) provide data to benchmark the out-of-pile ballooning and rupture data that have been used to establish cladding strain to failure criteria. The test rods were typical of PWR design except for a smaller length (0.91 m) and higher enrichment (12.5%). The fuel rod design is shown in Table 1. The axial power profile is shown in Figure 1. Transient coolant conditions were typical of the blowdown phase of a LOCA. Coolant pressure, mass flux, quality, and temperature at the midplane of the fuel rods are shown in Figures 2 to 5. Fuel rod power was typical of decay heat. The average power history is shown in Figure 6.

3.2 KfK FR2 G3 LOCA Experiment

An in-pile test on an array of fuel rods was carried out at the KfK Laboratory in Karlsruhe, W. Germany. The objectives of the test were: (a) provide qualitative and quantitative information on possible effects of a nuclear environment on the mechanisms of fuel rod failure under LOCA

TABLE 1. DESIGN OF TEST FUEL RODS FOR PBF-LOC-3 EXPERIMENT

Characteristic	Value
Active fuel length (m)	0.8788
Fuel rod outer diameter (cm)	0.993
Radius of pellet shoulder (mm)	3.3
Depth of pellet dish (mm)	0.343
Height of pellet (cm)	1.524
Pellet diameter (cm)	0.8534
Pellet density (% theoretical)	94.4959
Radial gap width (mm)	0.108
Number of coils in the plenum	17
Height of plenum spring (cm)	6.032
Outer diameter of spring (mm)	8.622
Spring wire diameter (mm)	1.02
Plenum volume (cm^3)	4.7
Fill gas	Helium
Fill gas pressure (MPa)	5.066
As fabricated fill gas temperature (K)	294

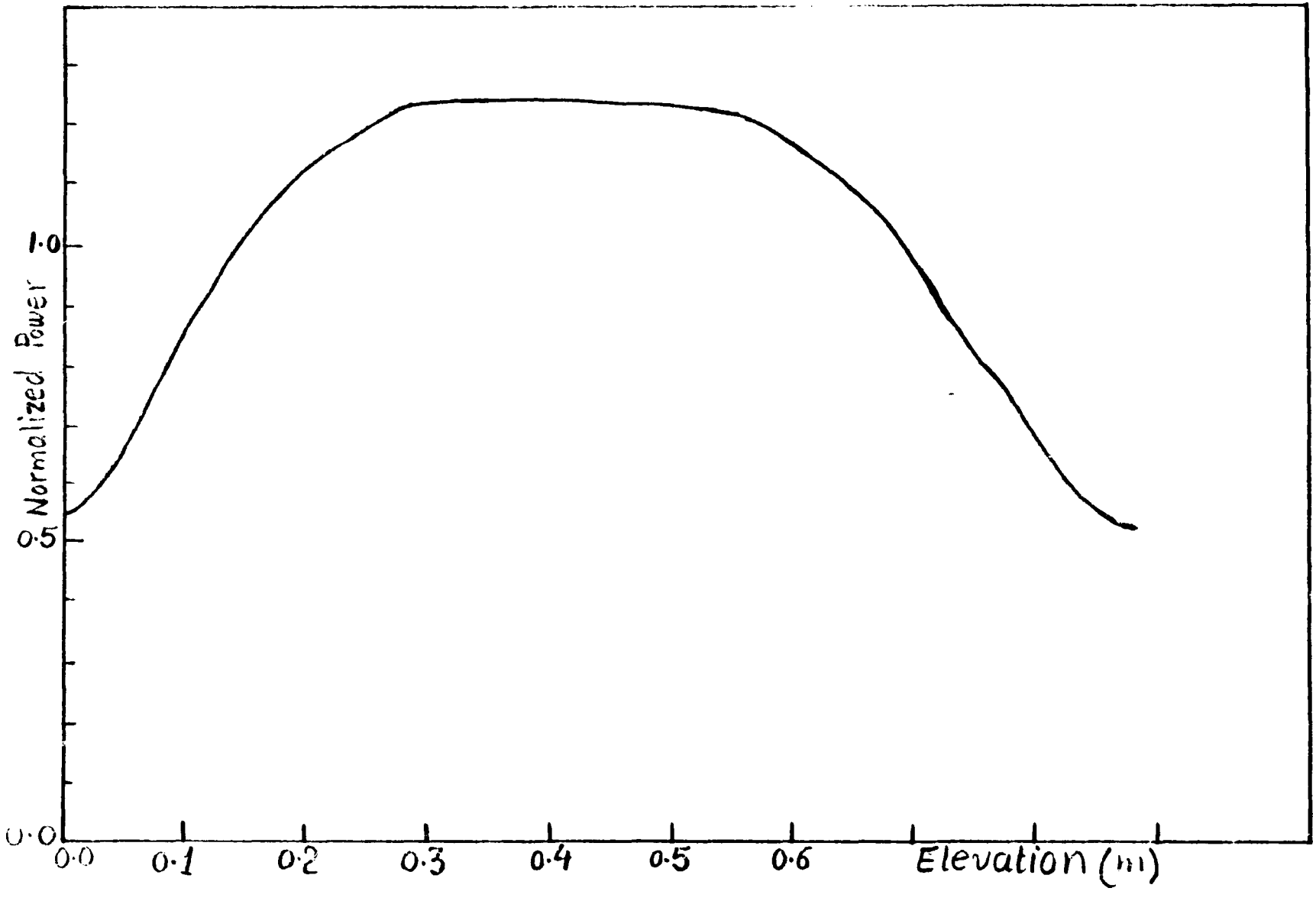

Figure 1. Axial power profile for PBF-LOC3 Test

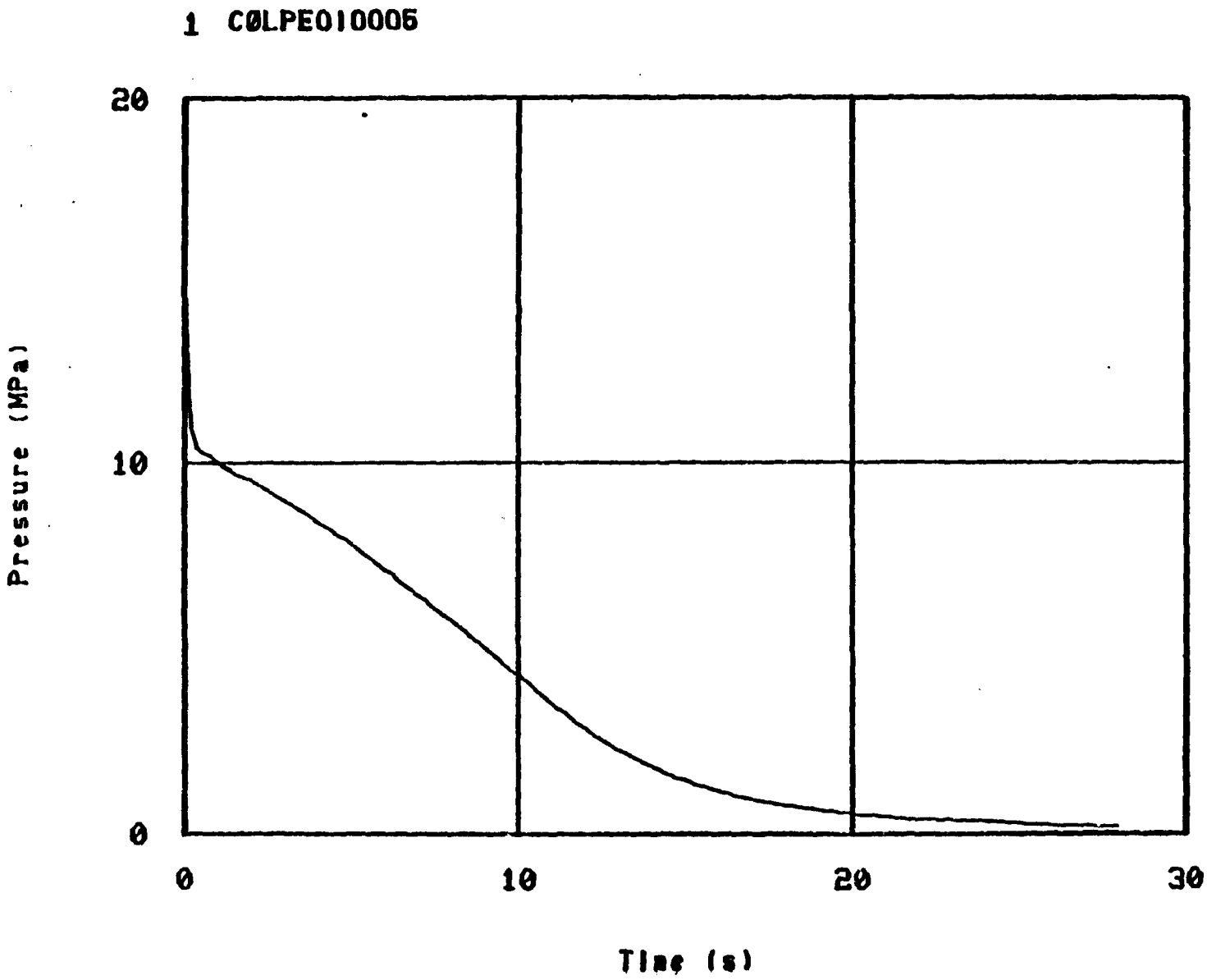

Figure 2. Coolant pressure as a function of time for PBF-LOC3 Test

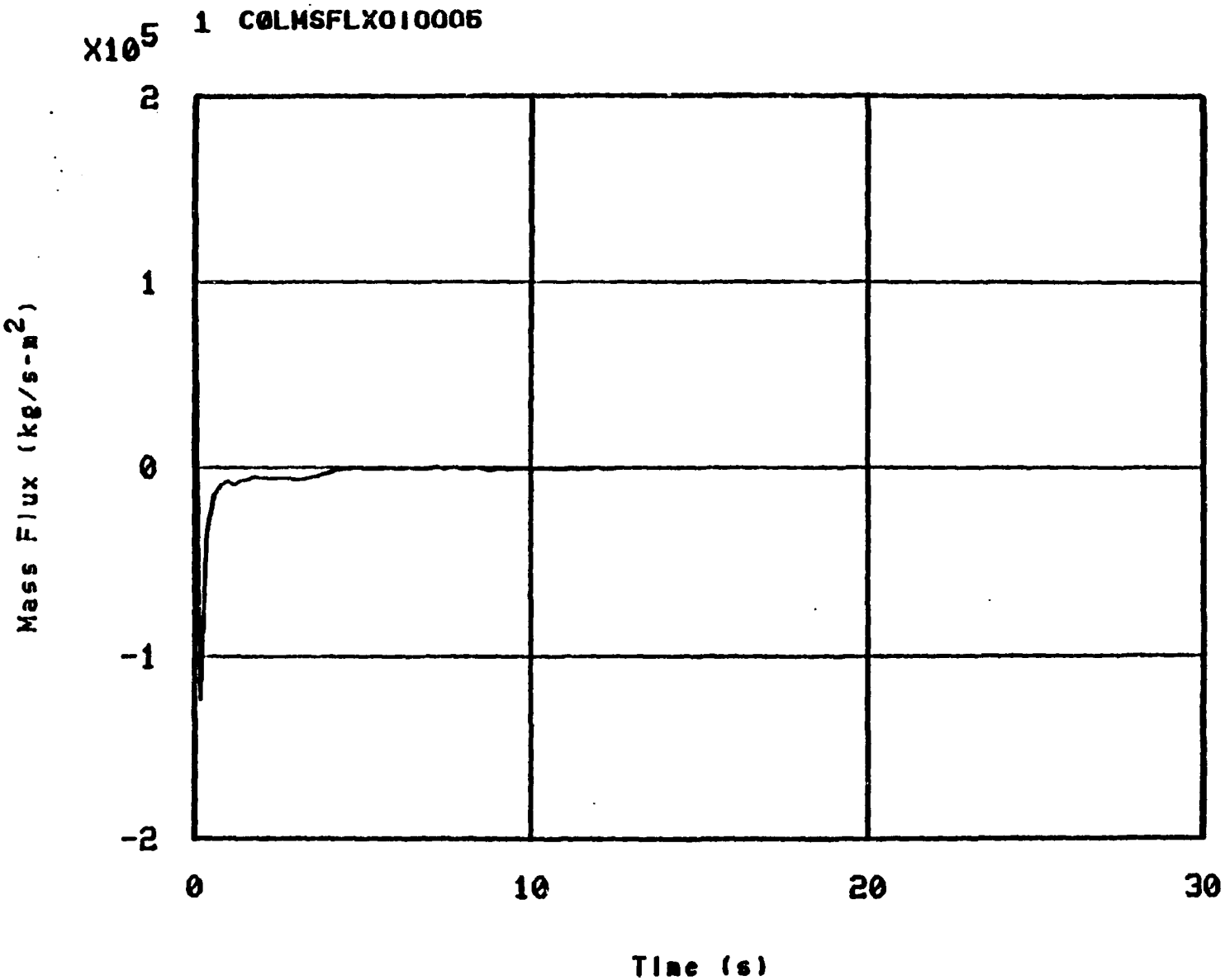

Figure 3. Coolant mass flux as a function of time for PBF-LOC3

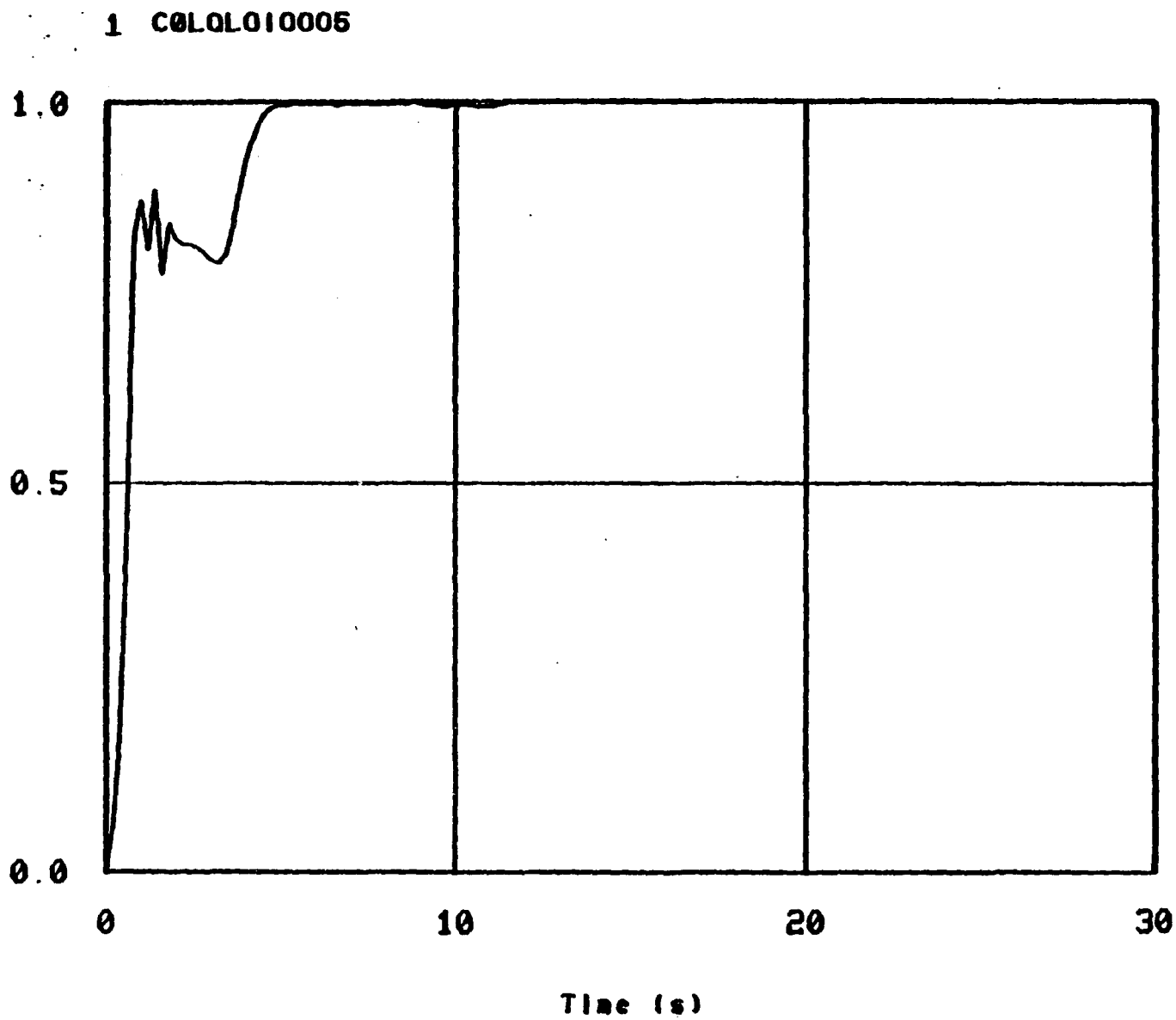

Figure 4. Coolant quality as a function of time for PBF-LOC3

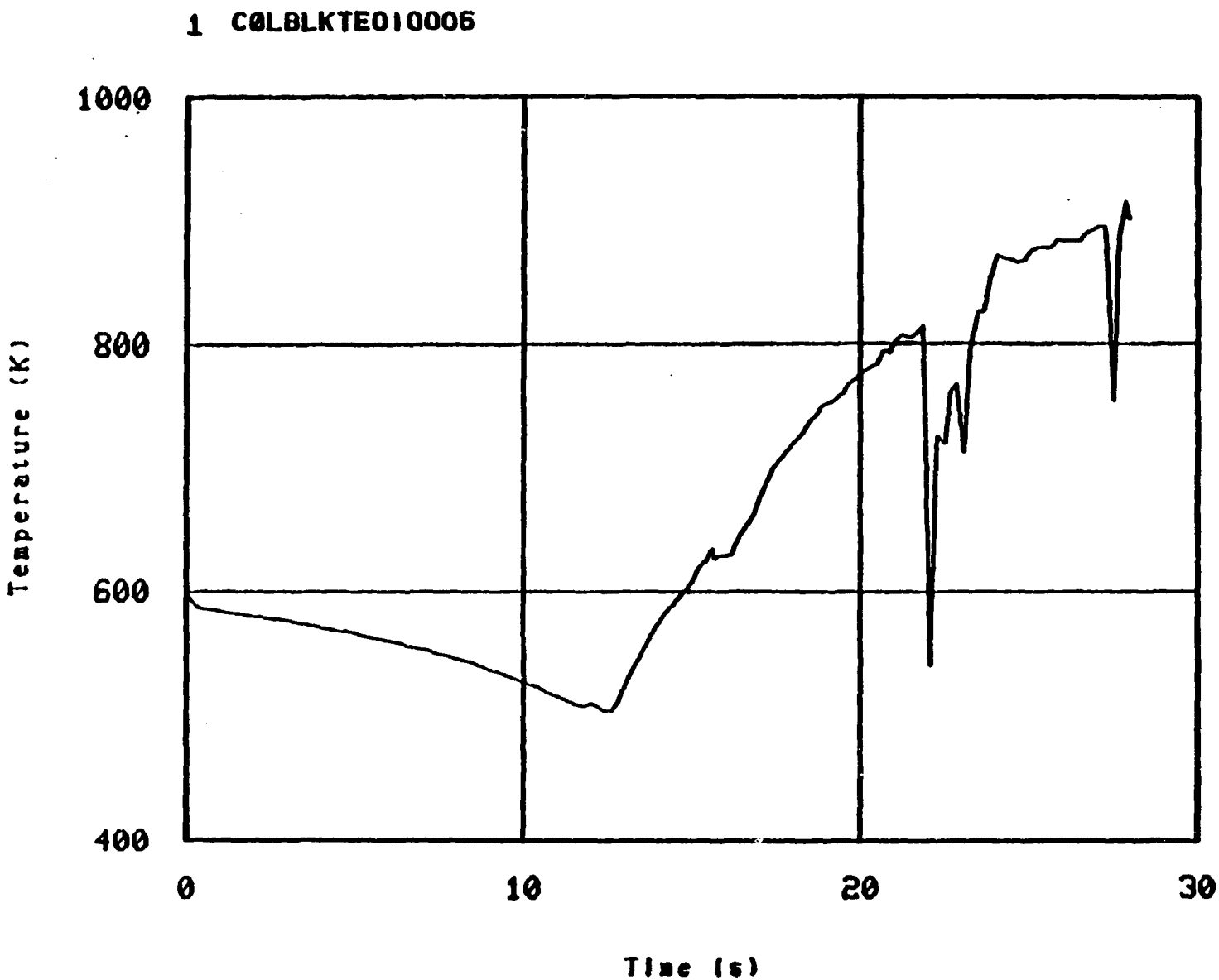

Figure 5. Coolant bulk temperature as a function of time for PBF-LOC3

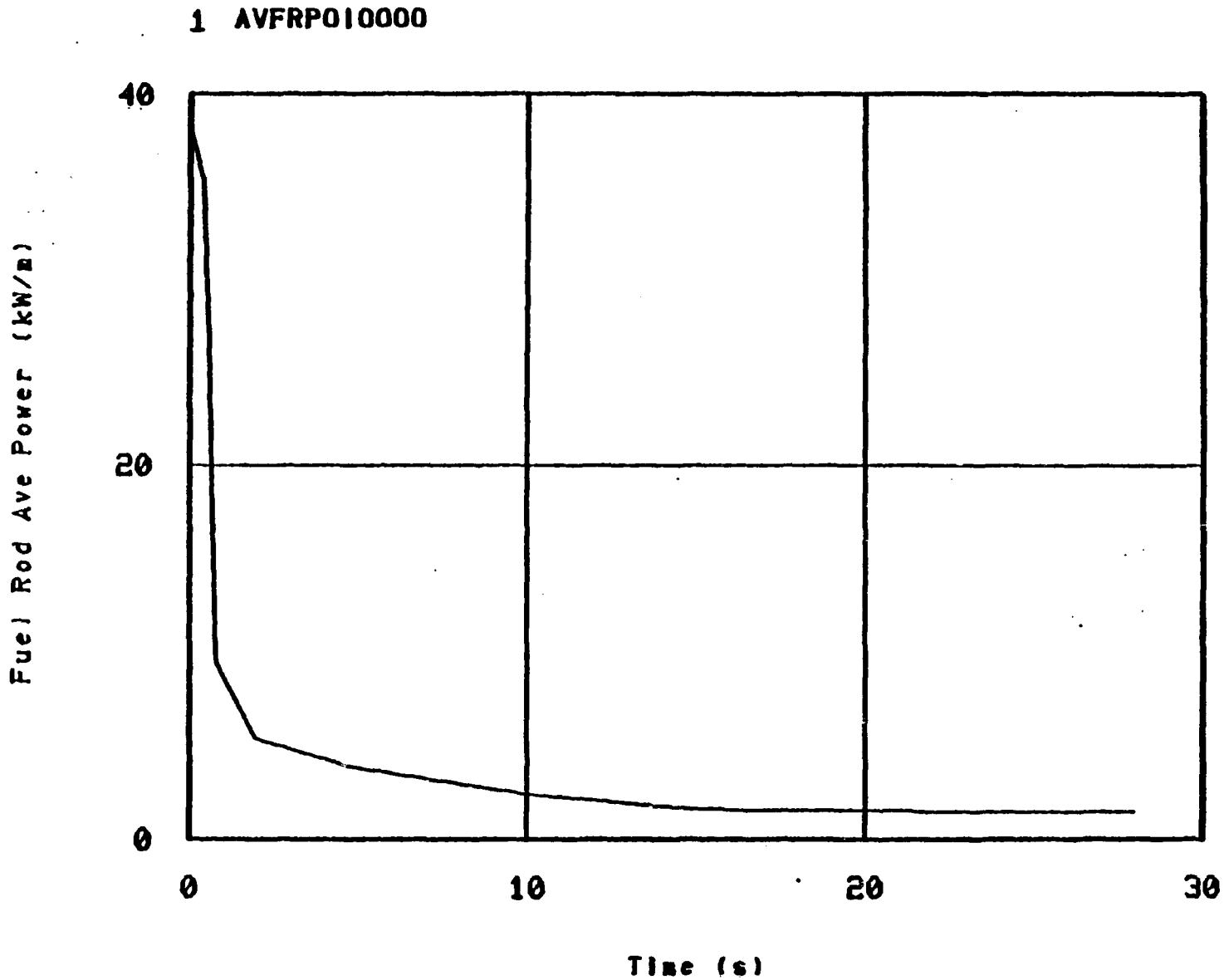

Figure 6. Average power as a function of time for PBF-LOC3

conditions; and (b) identify possible additional failure mechanisms. The test rod was a typical German PWR fuel design except for a smaller length (0.5 m) and a slightly higher enrichment (4.7%).

The rod was irradiated to a high burnup before the test. The fuel rod design is shown in Table 2 and the coolant pressure, cladding temperature, average power and axial power profile are shown in Figures 7 to 10.

3.3 The International Standard Problem (ISP 19)

An experiment on a 5 x 5 array of fuel rods was carried out in the Phebus reactor at Cadarache, France and presented as a potential standard problem in June 1984. In this test a bundle of nuclear fuel rods were subjected to a fast transient corresponding to a large break accident in a pressurized water reactor. The test rods had a typical PWR design except for a shorter length (0.8 m). The fuel rod design is shown in Table 3 and the axial power profile, coolant temperature, coolant pressure, surface heat transfer coefficient and the average power are shown in Figures 11 to 15.

3.4 TREAT FRF-2 Fuel Rod Failure Test

This test was carried out in the Transient Reactor Test Facility (TREAT) at INEL using a seven-rod bundle of 0.635 m long fuel rods in a flowing steam atmosphere. The design of the test rods is shown in Table 4. The LOCA accident was simulated by operating the TREAT reactor so that the fission heat in the UO_2 pellets caused the Zircaloy cladding temperature to increase at a rate of 24 k/s to a maximum temperature of approximately 1590 K. The fuel rods were initially pressurized with helium to a pressure of 0.45 to 0.52 MPa to simulate accumulated fission gases.

The coolant bulk temperature, pressure and mass flux are shown in Figures 16 to 18, the average power is shown in Figure 19 and the axial power profile is shown in Figure 20.

The specification of the boundary conditions for the four tests are summarized in Table 5.

TABLE 2. DESIGN OF TEST FUEL RODS FOR KfK FR2 EXPERIMENT

Characteristic	Value
Cladding	
Material	Zircaloy-4
Outside diameter, mm	10.75
Inside diameter, mm	9.3
Wall thickness, mm	0.725
Fuel Pellets	
Material	UO_2
Diameter (nominal gap), mm	9.11
Diameter (small gap), mm	9.15
Length, mm	11
Burnup, MWd/t	32,000
Enrichment (active zone), %	4.7
Enrichment (end pellets), %	0.3
Height of pellet stack (active zone), mm	500
Density, G/cm^3	10.35
Theoretical density, %	94.4
Insulating Pellets	
Material	Al_2O_3
Diameter, mm	9.15
Length, mm	8
Void Volumes	
Dishing per pellet, mm^3	16
Gap volume (nominal gap), cm^3	1.57
Total plenum volume (including pressure transducer), cm^3	28.12
Fill gas composition	100% helium
Fill gas pressure (MPa)	5

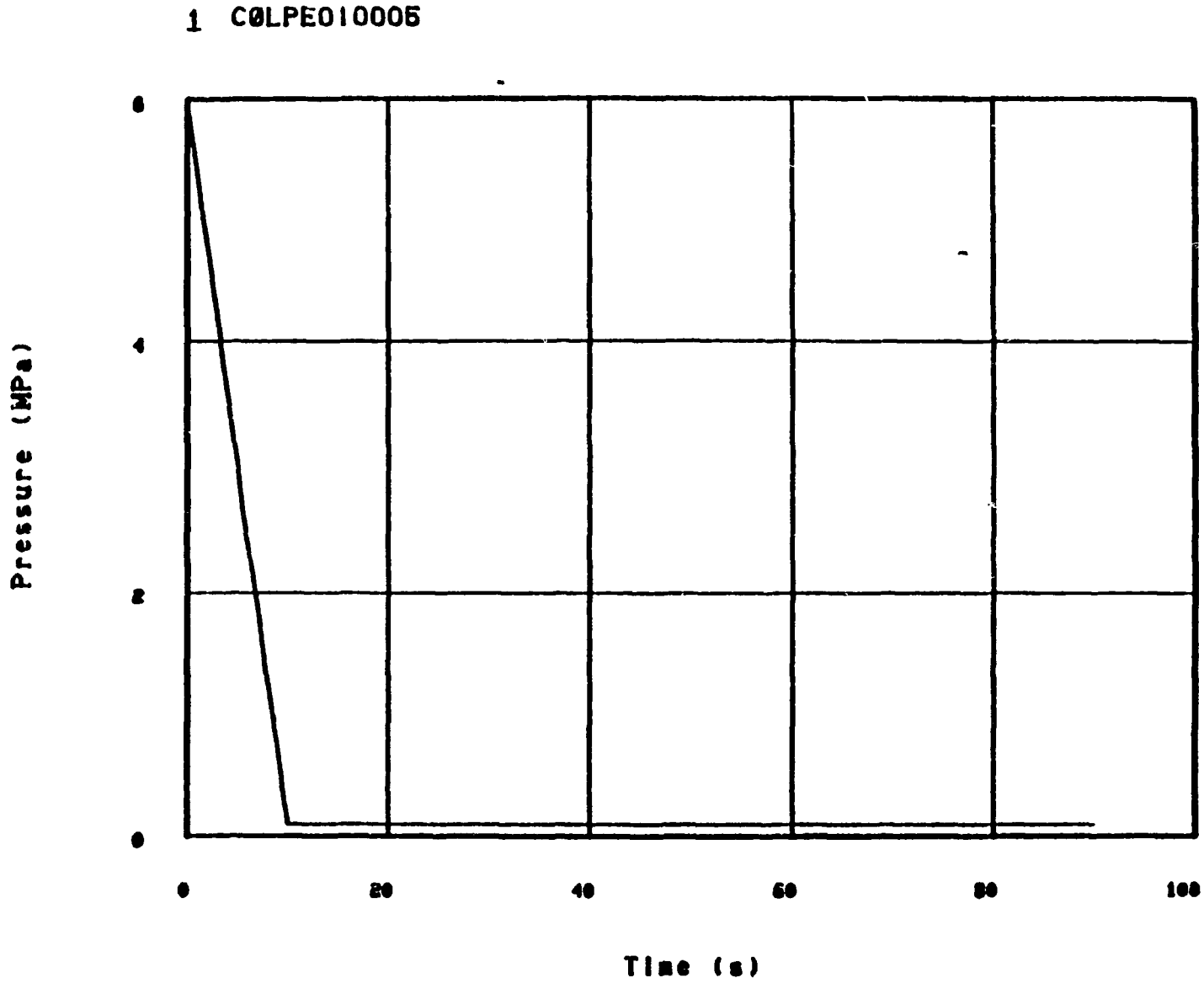

Figure 7. Coolant pressure as a function of time for KfK

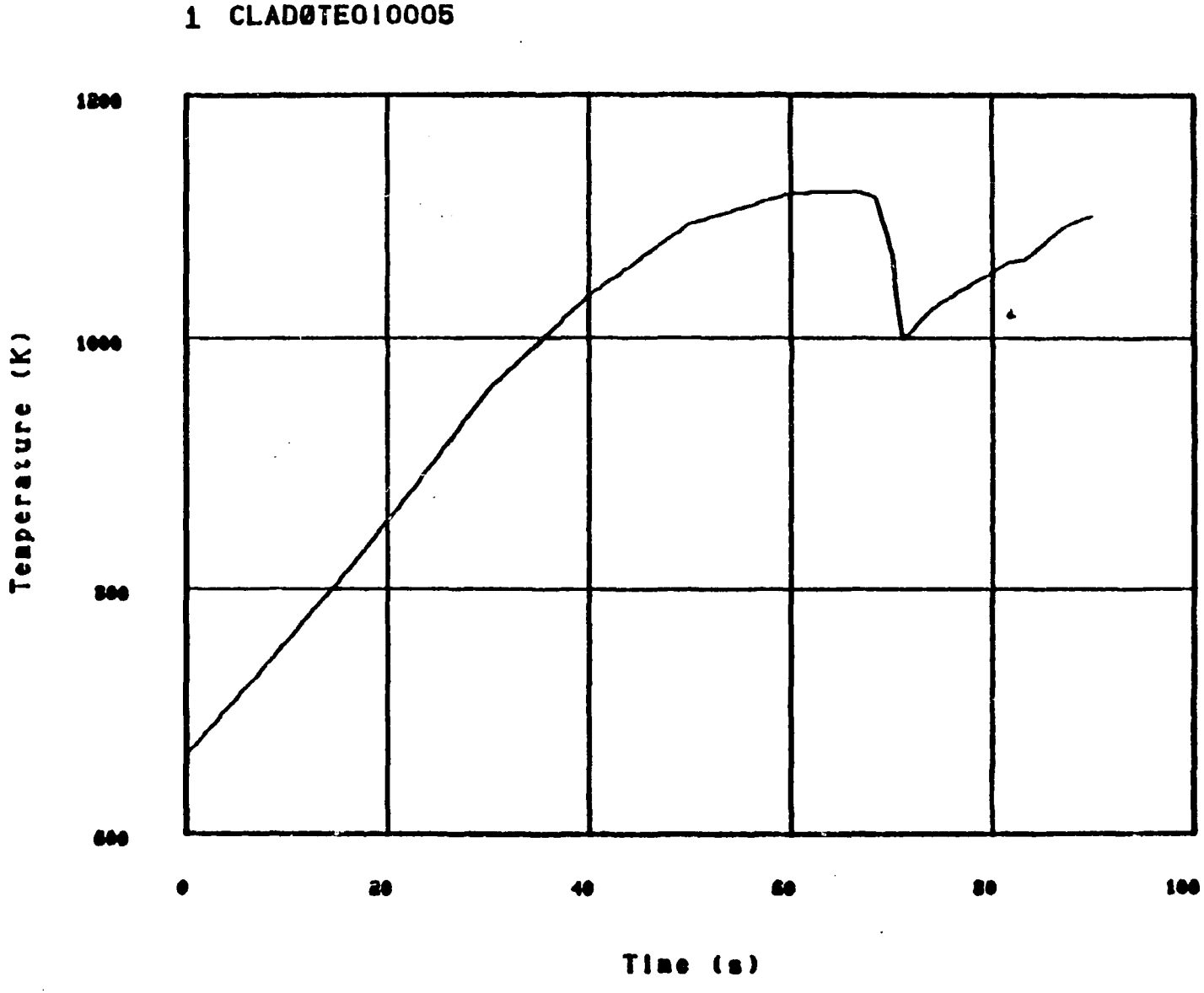

Figure 8. Cladding temperature ~~Coolant pressure~~ as a function of time for KfK

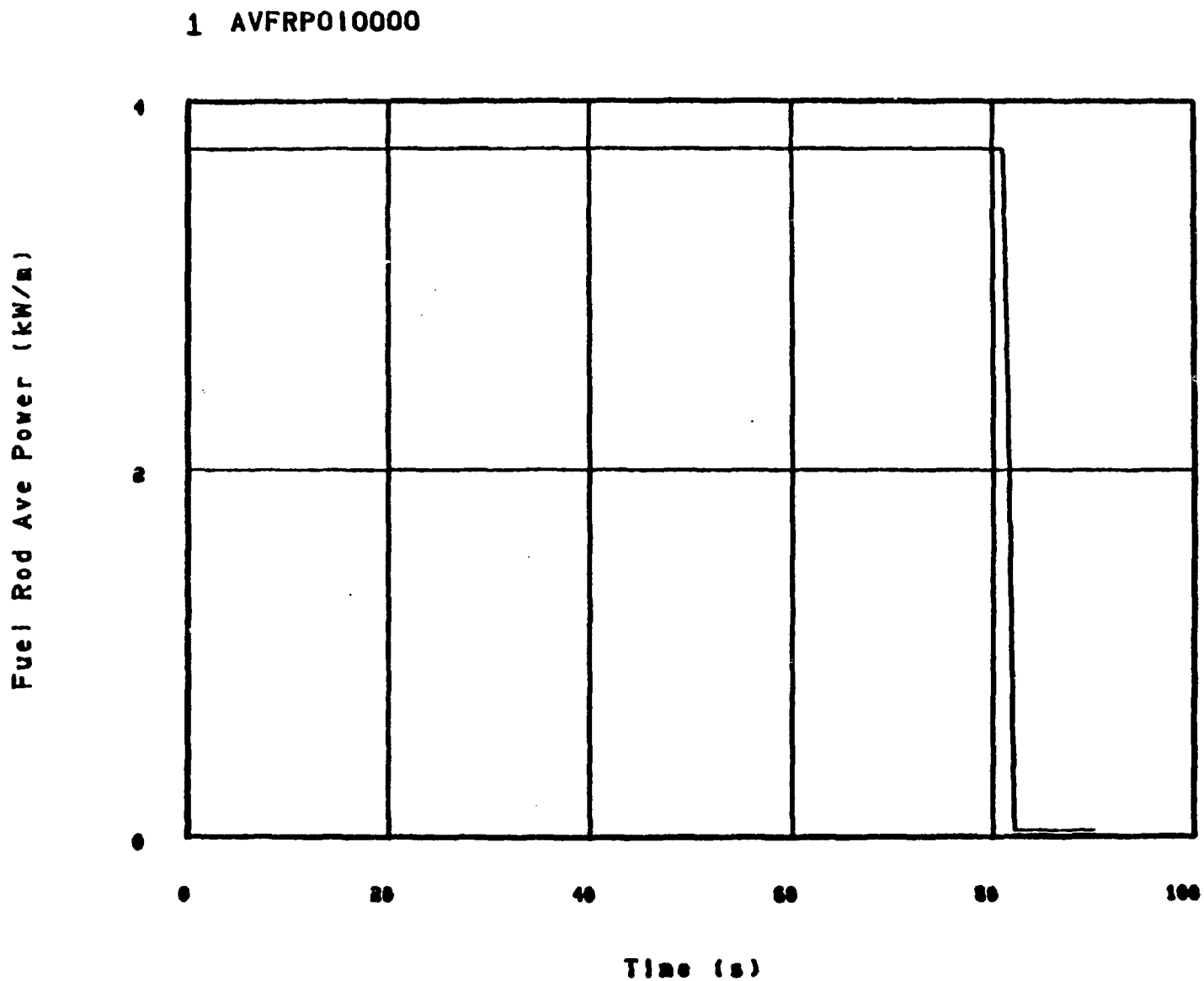

Figure 9. Average power as a function of time for KfK

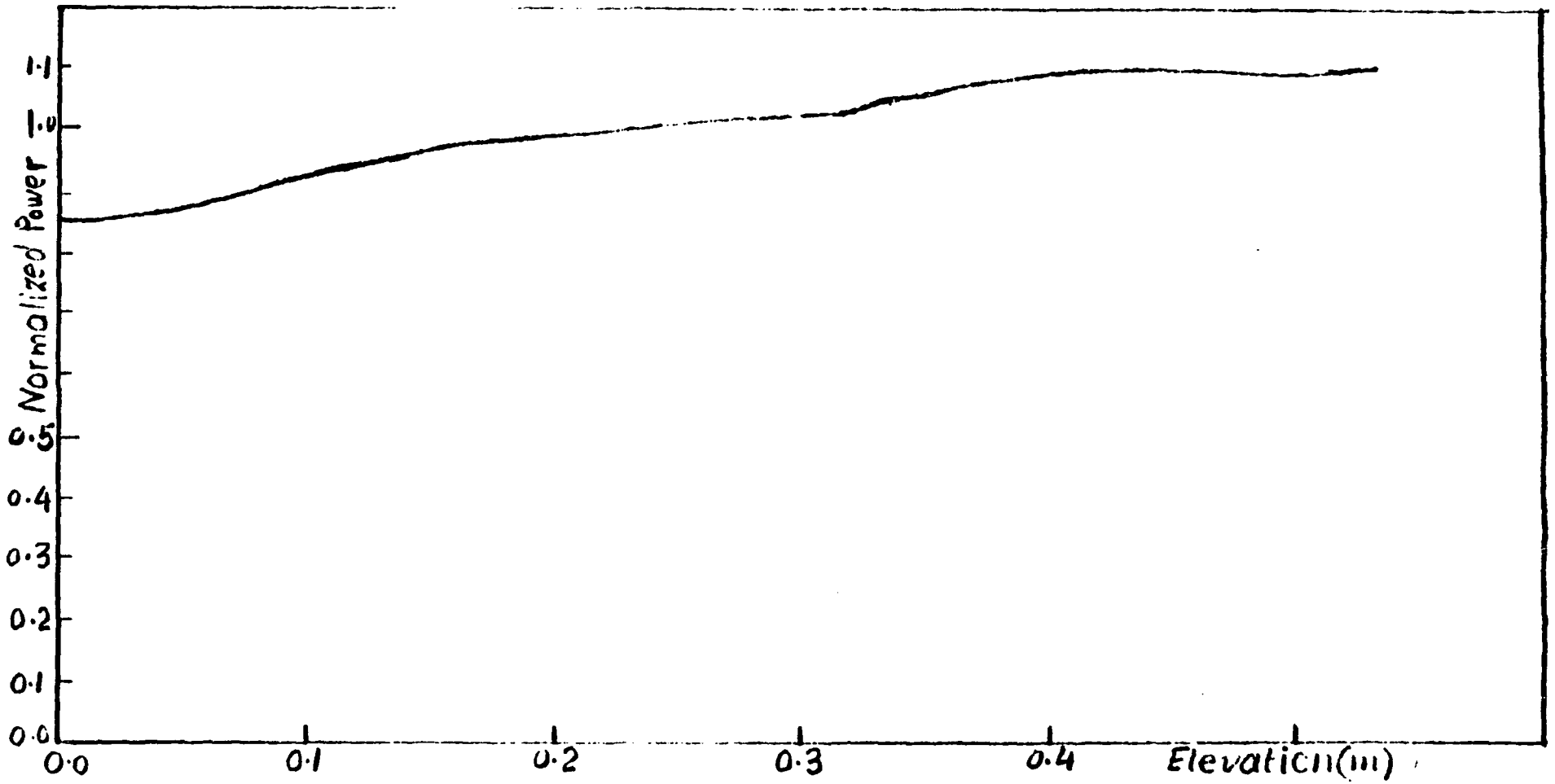

Figure 10. Axial power profile for KfK

TABLE 3. DESIGN OF TEST FUEL RODS FOR PHEBUS TEST

Fuel rod length (m)	0.8
Fuel rod outer diameter (cm)	0.956
Height of pellet (cm)	1
Pellet diameter (cm)	0.819
Pellet density (% theoretical)	94
Radial gap (mm)	0.85
Number of coils in the plenum spring	20
Spring height (m)	0.2
Outer diameter of spring (cm)	0.82
Wire diameter of spring (mm)	2
Fill gas	Helium
Fill gas pressure (MPa)	8.88
As fabricated fill gas temperature (K)	298

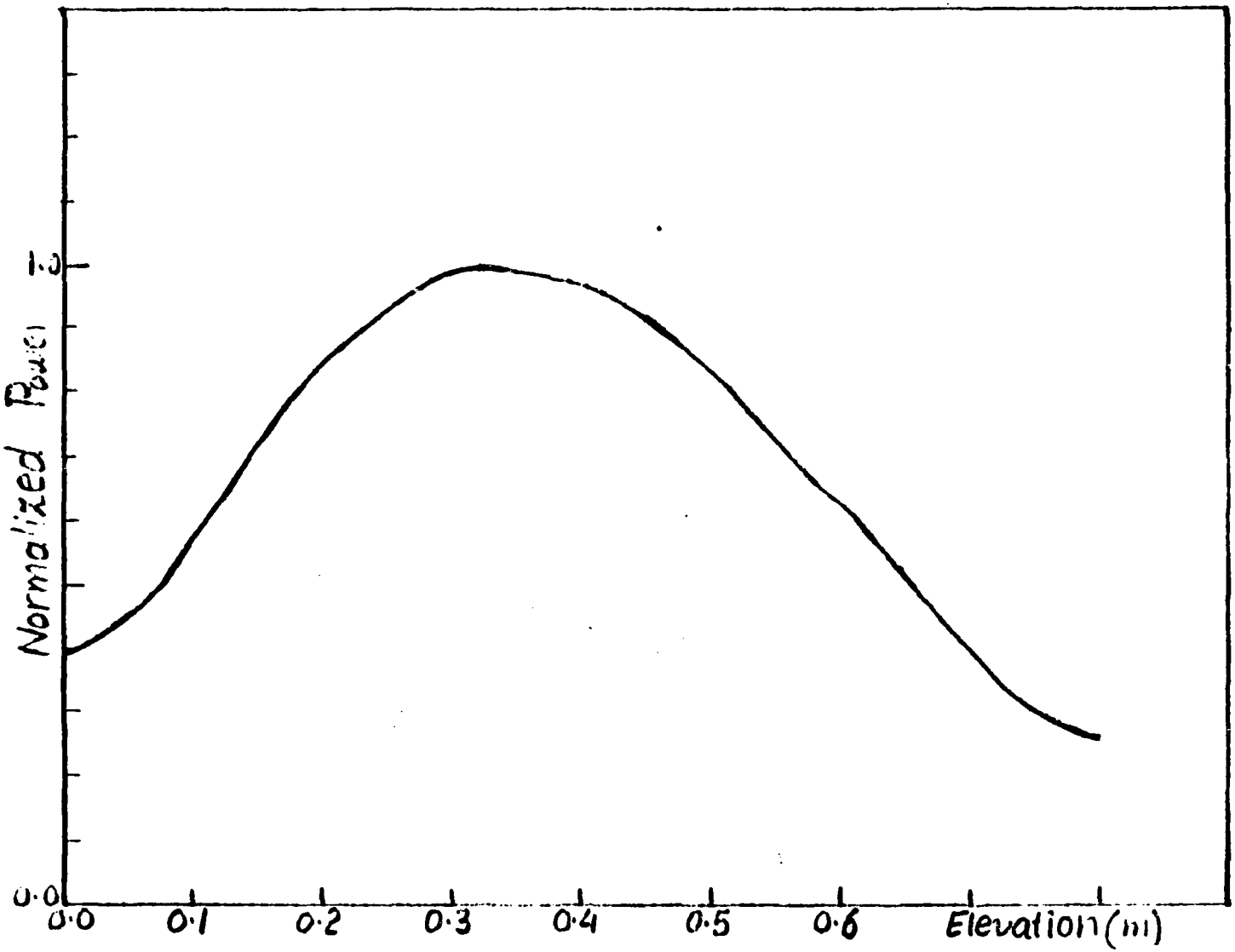

Figure 11. Axial power profile for Phebus

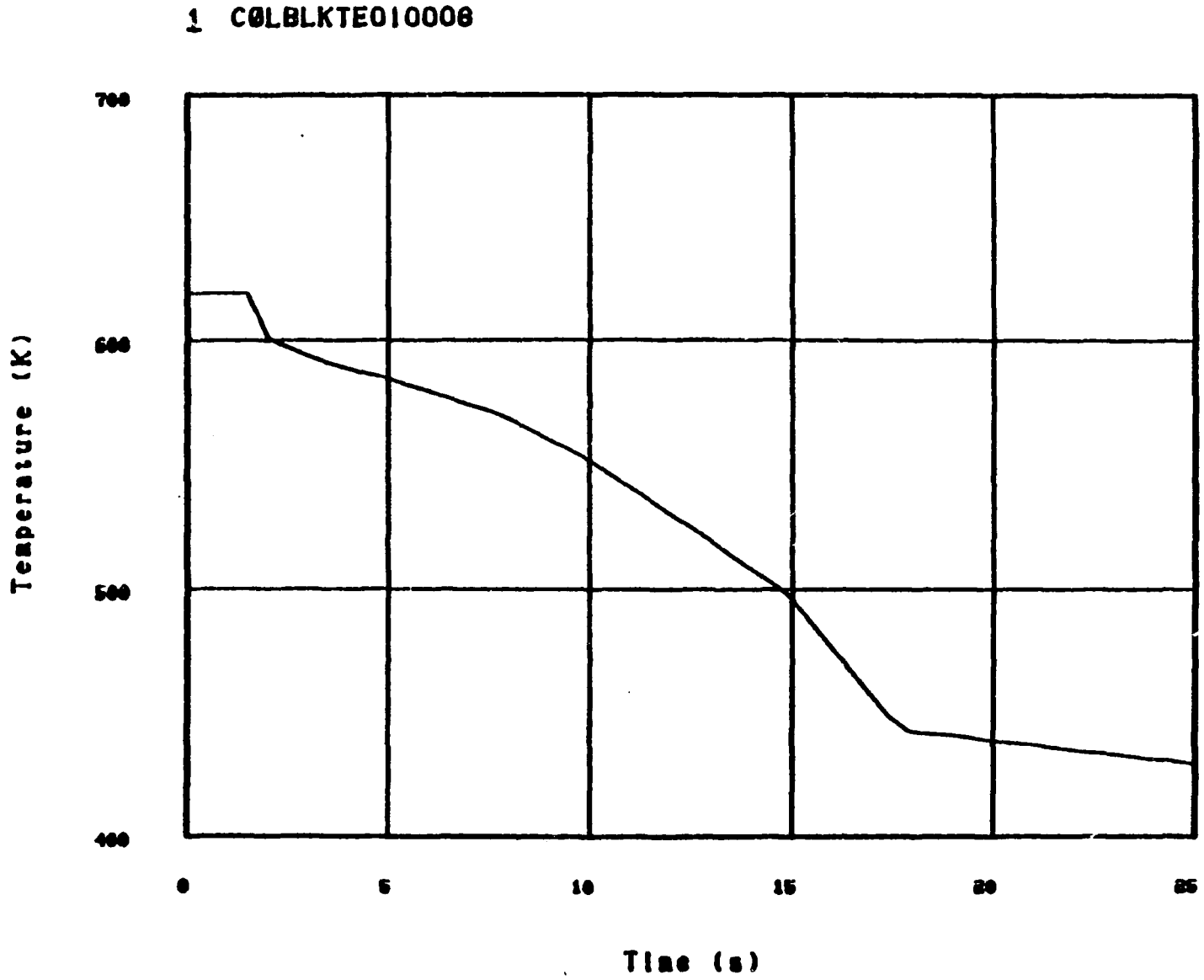

Figure 12. Coolant temperature as a function of time for Phebus

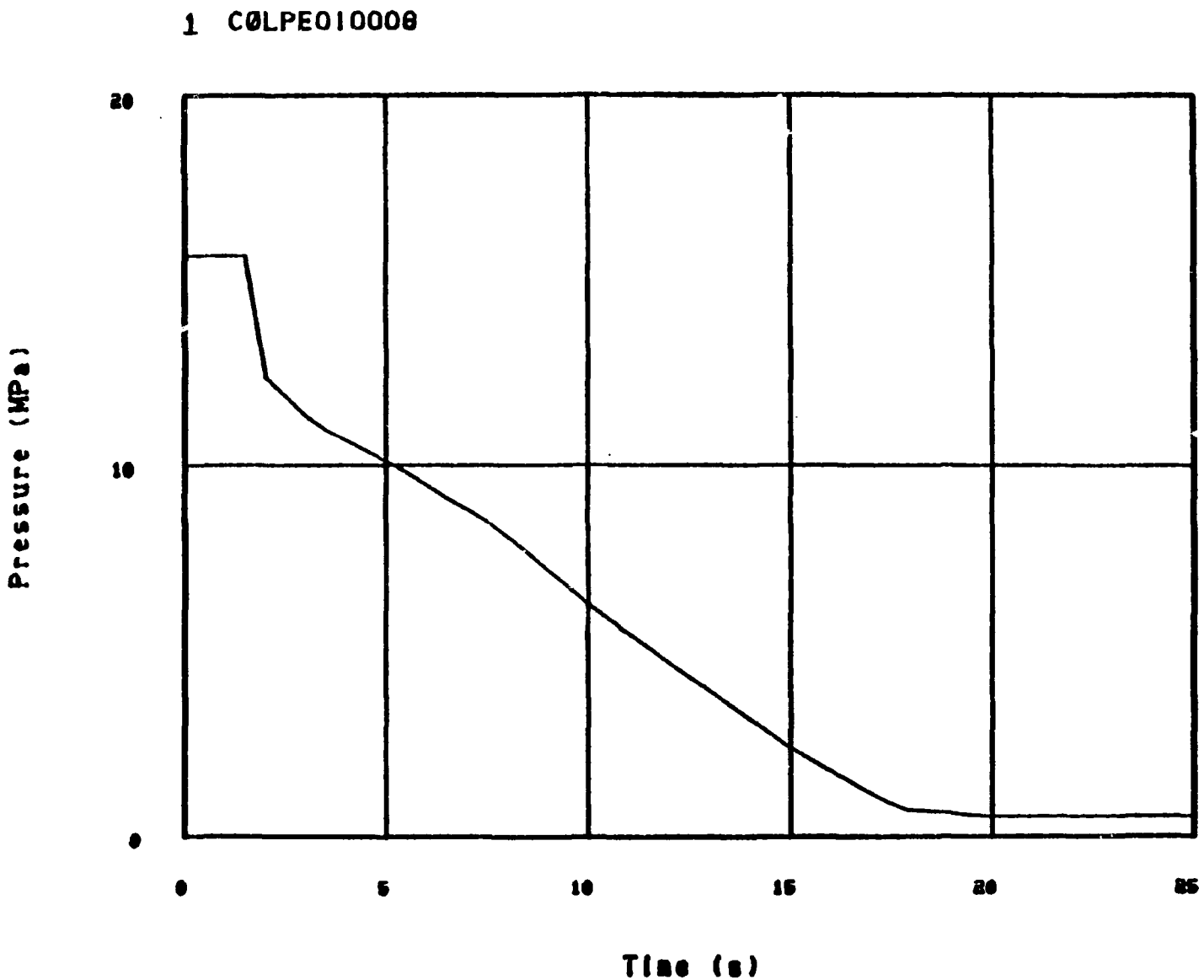

Figure 13. Coolant pressure as a function of time for Phebus

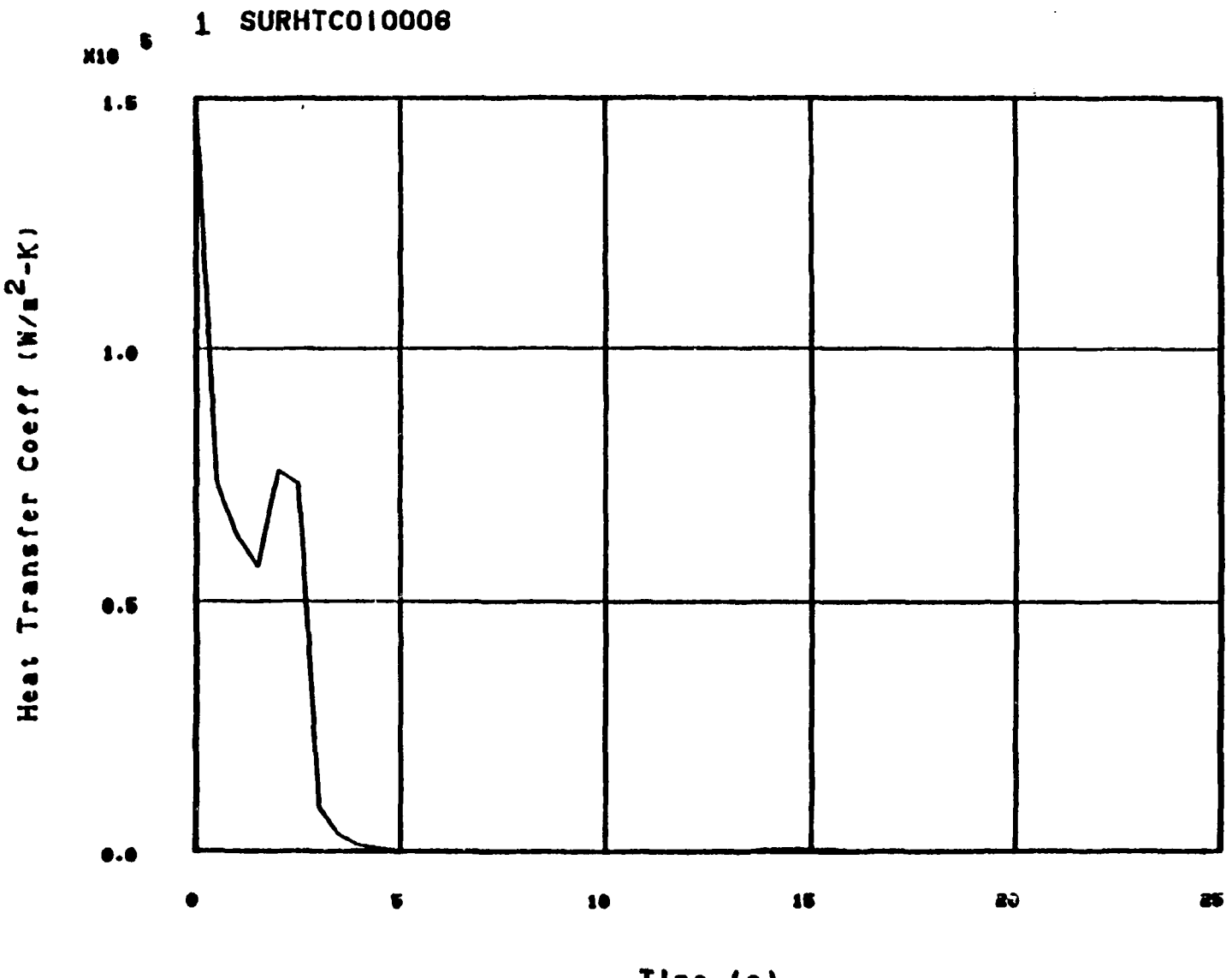

Figure 14. (a) Surface heat transfer coefficient as a function of time for Phebus

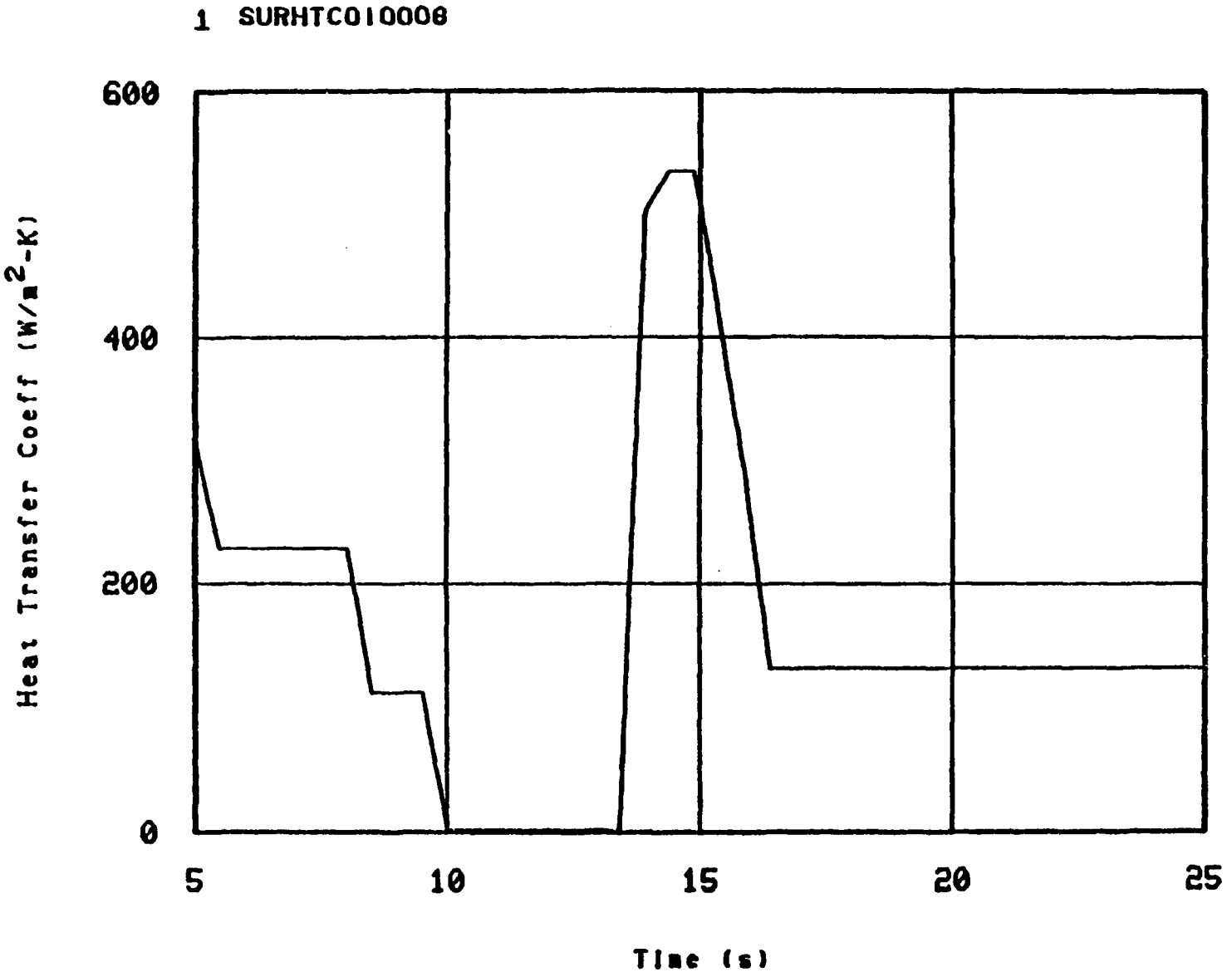

Figure 14. (b) Surface heat transfer coefficient as a function of time for Phebus (Zone after 5 seconds being magnified)

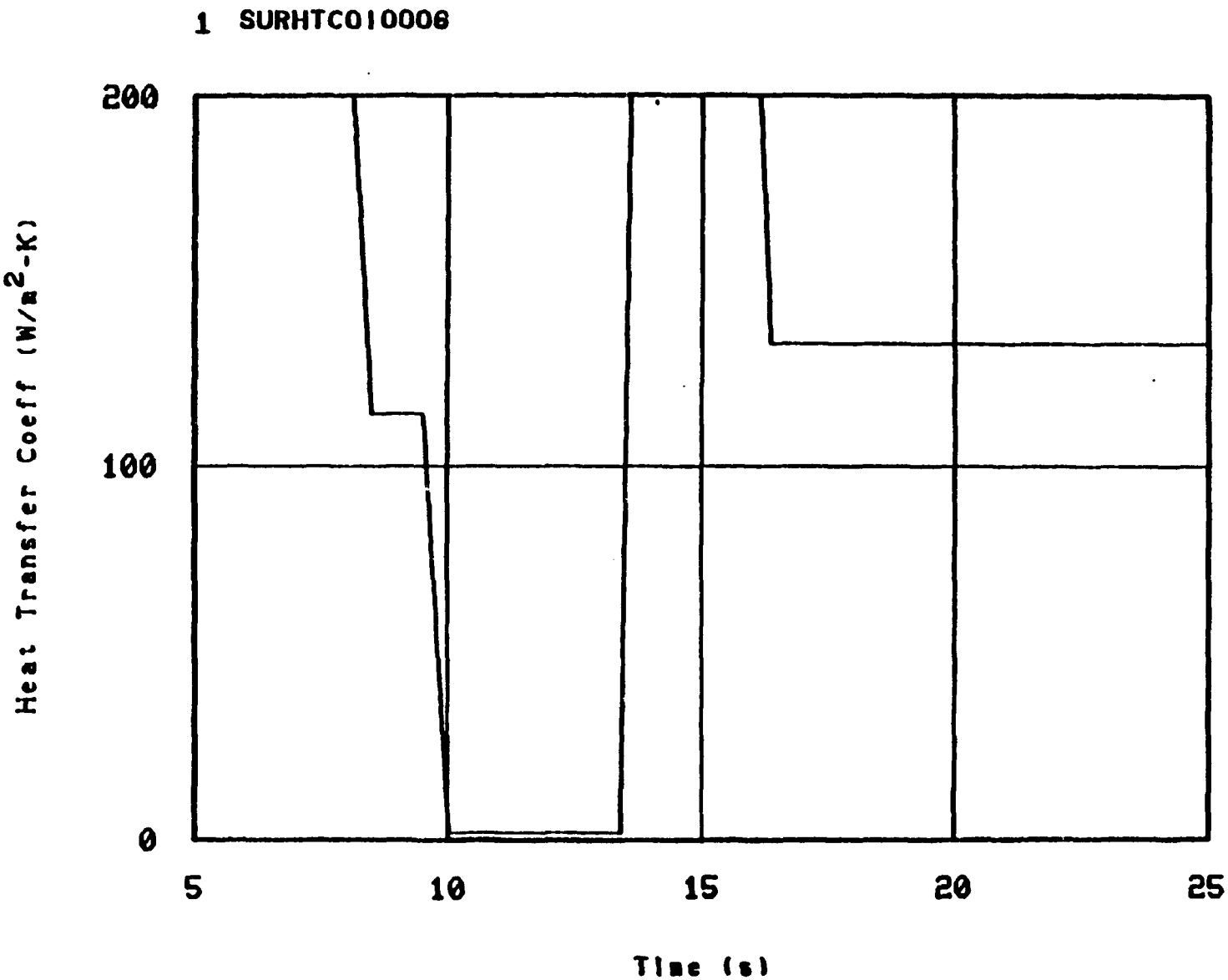

Figure 14. (c) Surface heat transfer coefficient as a function of time for Phebus (Zone after 5 seconds being more magnified)

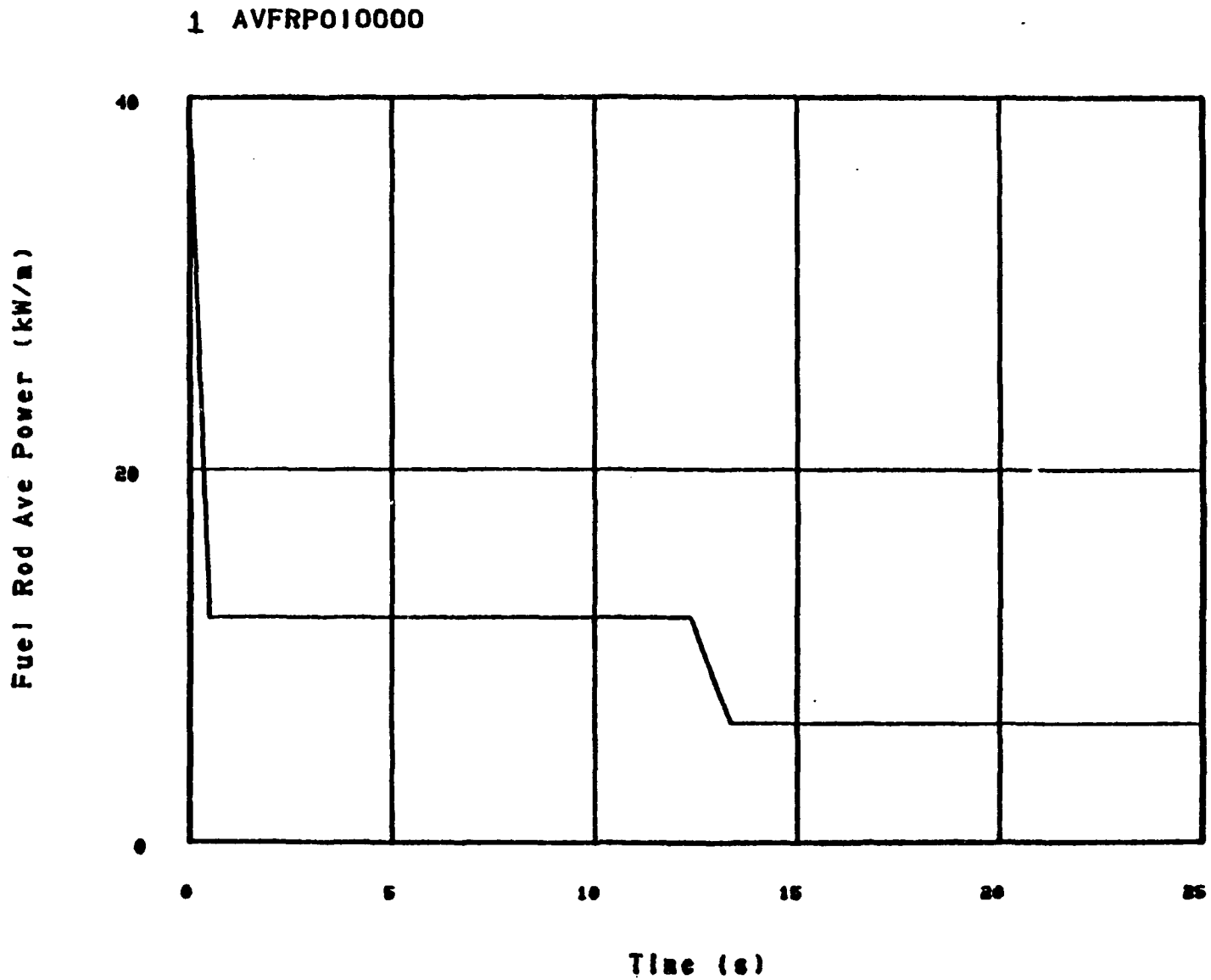

Figure 15. Average power as a function of time for Phebus

TABLE 4. DESIGN OF TEST FUEL RODS FOR TREAT TEST

Active fuel length (m)	0.635
Outer diameter of cladding (cm)	1.43
Radius of pellet shouider (cm)	0.415
Pellet height (cm)	3.048
Pellet diameter (cm)	1.256
Pellet density (% theoretical)	95
O/U ratio	2
Radial gap width (M)	61.5
Number of coils of the plenum spring	20
Height of the spring (cm)	6.032
Diameter of the spring (cm)	0.902
Diameter of the spring wire (cm)	0.1042
Fill gas	Helium
Fill gas pressure (MPa)	0.52
As fabricated fill gas temperature (K)	298

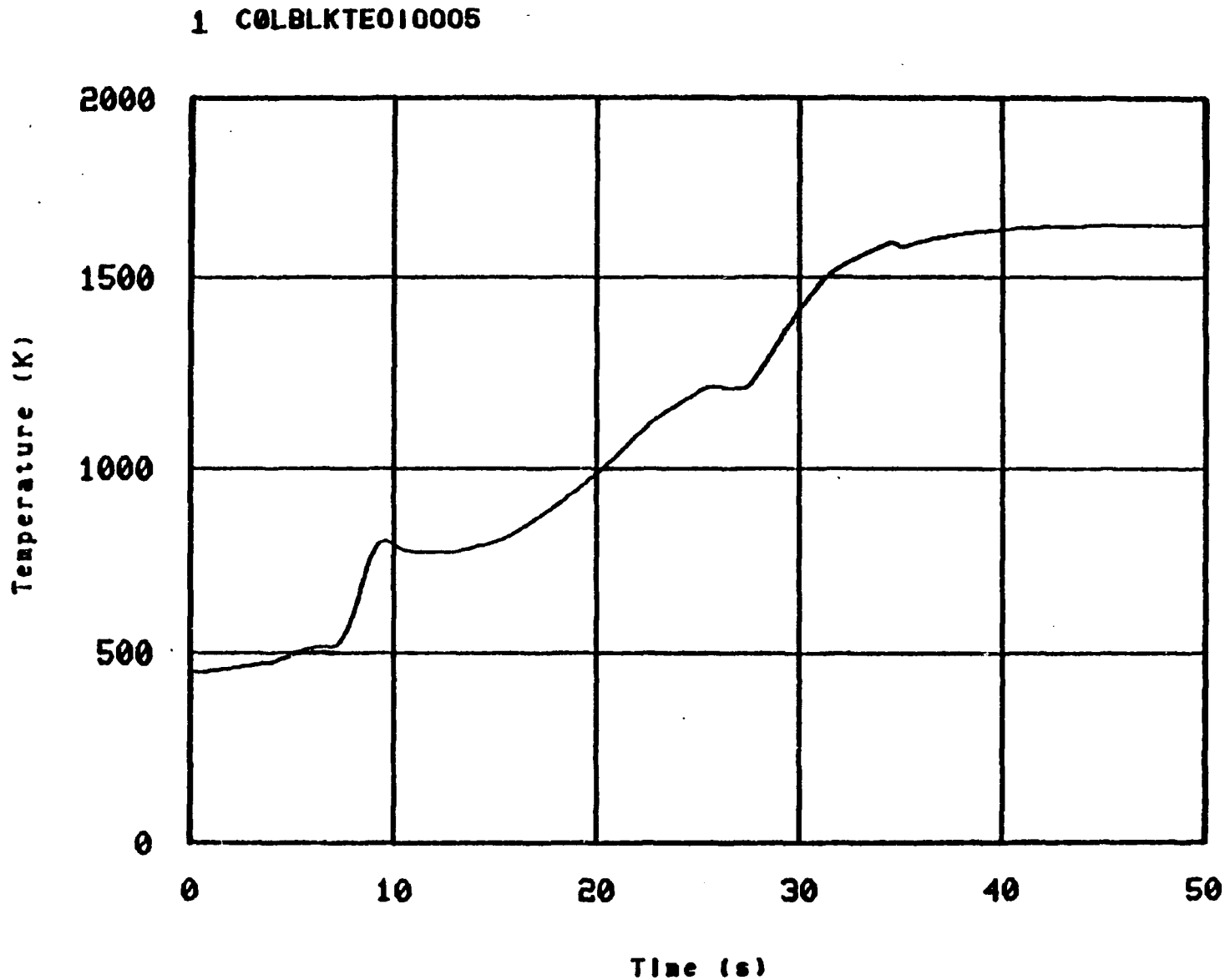

Figure 16. Coolant temperature as a function of time for TREAT

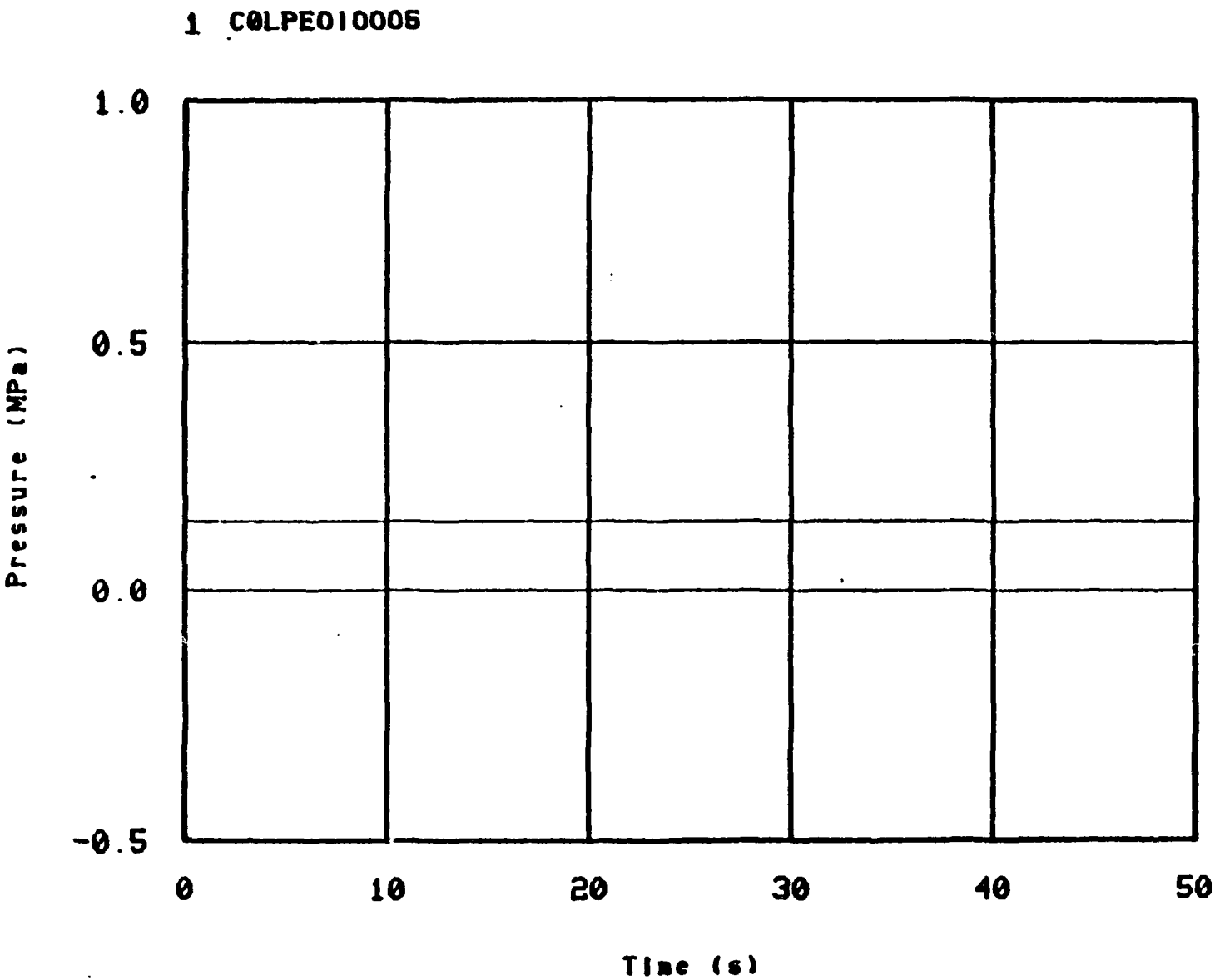

Figure 17. Coolant pressure as a function of time for TREAT

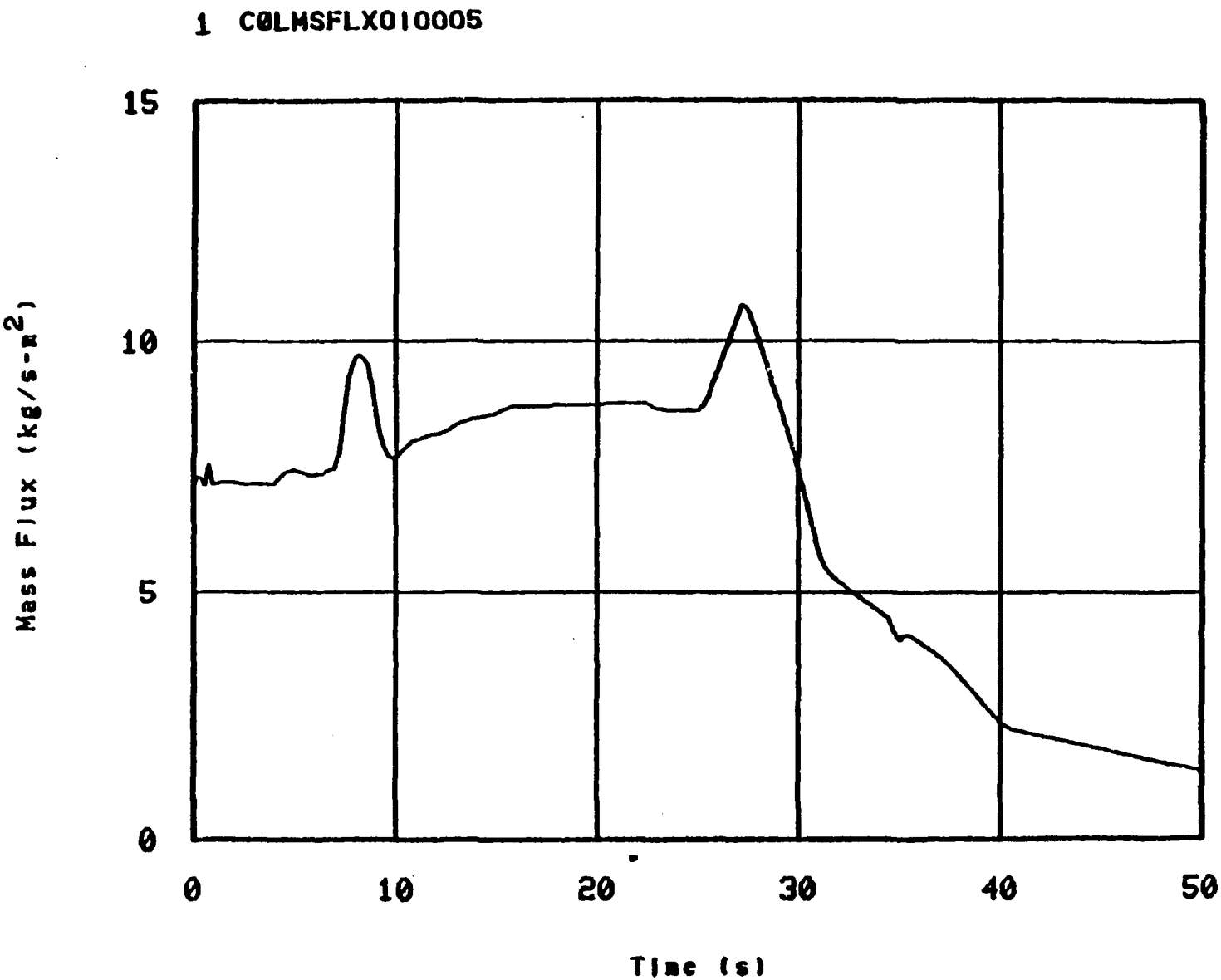

Figure 18. Coolant mass flux as a function of time for TREAT

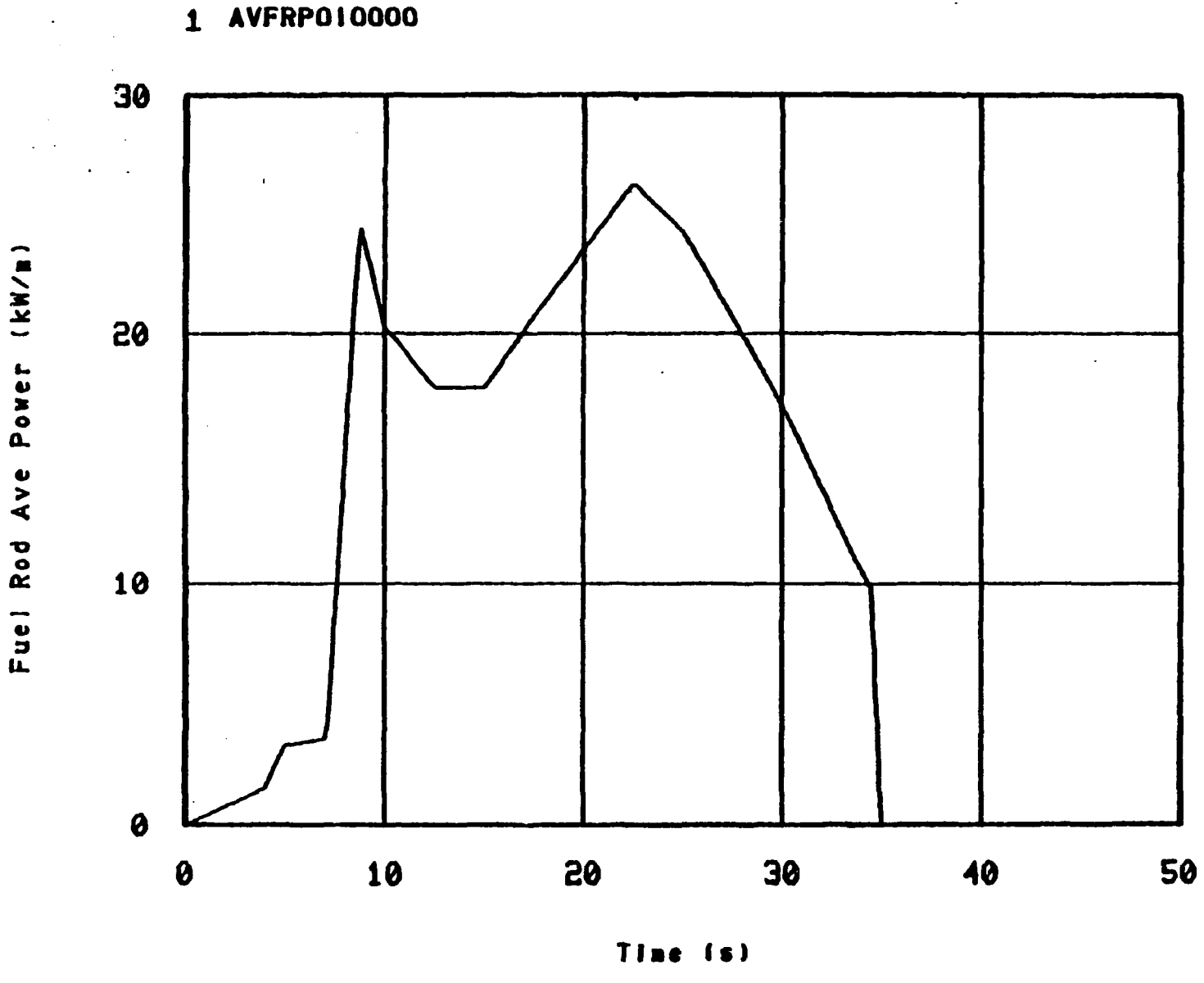

Figure 19. Average power as a function of time for TREAT

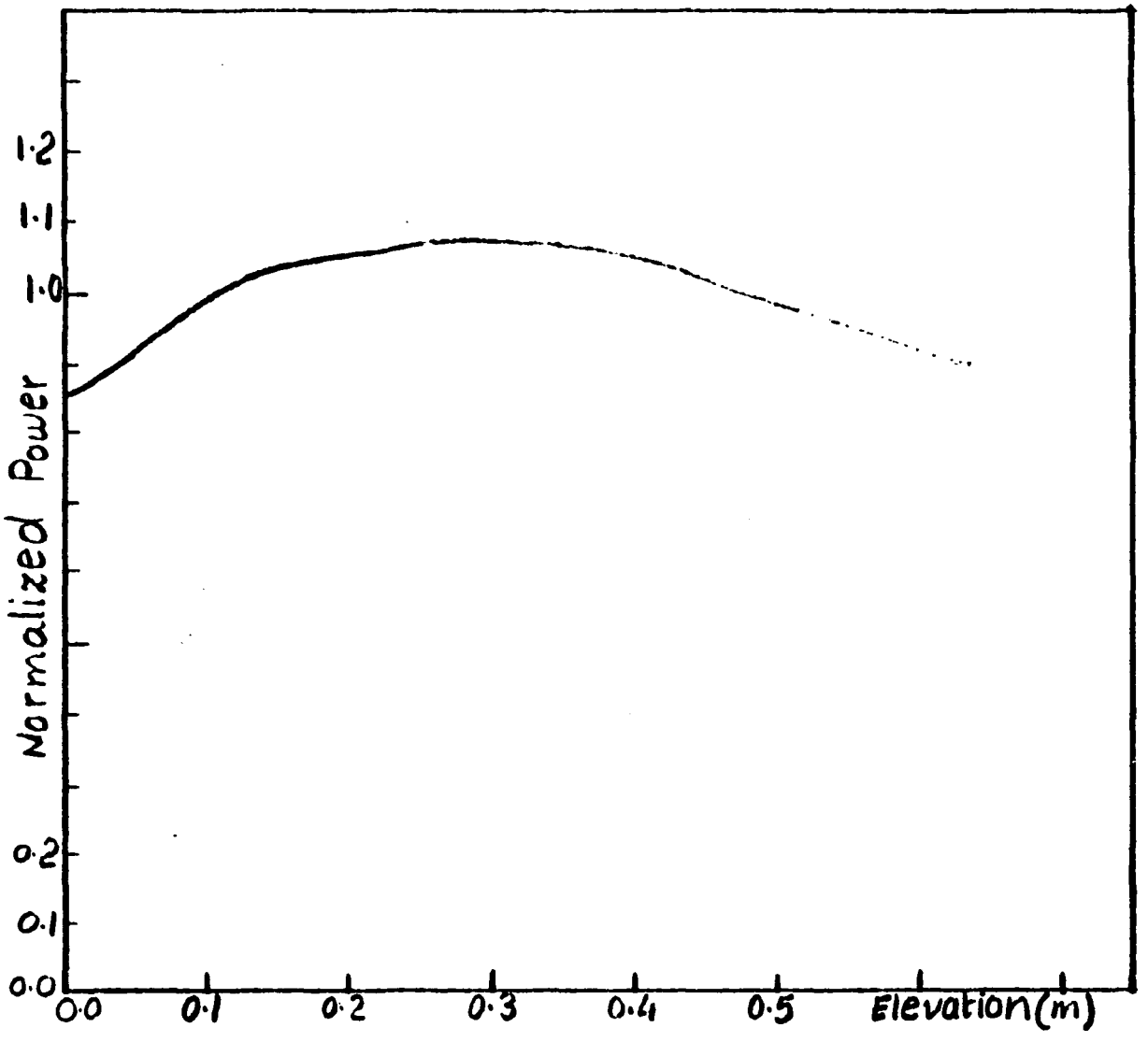

Figure 20. Axial power profile for TREAT

TABLE 5. METHOD OF SPECIFYING BOUNDARY CONDITIONS FOR THE FOUR TESTS

Test	Methods of Specifying Boundary Conditions
PBF LOC-3	Input of the local coolant conditions (pressure, mass flux, quality) that were calculated by RELAP5[13] code. FRAP-T6 calculated the local heat transfer coefficients.
KfK G3	Input of measured cladding surface temperature and coolant pressure.
Phebus 291	Input of the local heat transfer coefficients, coolant temperature and pressure that were calculated by RELAP5.
TREAT FRF-2	Input of measured inlet steam temperature, mass flux and bundle pressure. FRAP-T6 calculated the local coolant conditions and heat transfer coefficients.

4. ASSESSMENT OF BALLOONING MODEL

Each of the four ballooning experiments described in Section 3 was calculated with the FRAP-T6 code using the extended BALON2 model. Comparisons were then made of the calculated and measured characteristics of ballooning. The characteristics that were compared included: (a) time of cladding rupture, (b) maximum cladding hoop strain, and (c) axial profile of cladding hoop strain.

The FRAP-T6 code allows the code user to specify the boundary conditions for fuel rods by several different methods. At one extreme, the inlet coolant conditions can be specified and the code will calculate the transient conditions of the coolant surrounding the fuel rod and the transient cladding temperature. This method can only be used when the inlet coolant conditions are changing slowly, such as for the TREAT FRF-2 test. At the other extreme, the measured cladding temperatures are input and no calculation is made of the coolant conditions or the cladding temperature. Since cladding ballooning is sensitive to cladding temperature, the boundary conditions for each experiment were specified by the method that provided the smallest discrepancy between measured and calculated cladding temperature. If cladding temperatures were measured at almost all elevations of the fuel rod, then the measured cladding temperatures were input. Otherwise, the coolant conditions were either input to the code or calculated by the code and then the cladding temperatures were calculated. The method used to specify the boundary conditions for each of the four experiments is summarized in Table 5.

4.1 Effect of Extensions to the Ballooning Model on the Rupture Time

The calculated values of the rupture time are compared in Table 6 to the measured values. The calculated times include those with and without the extensions ballooning model. It can be seen that in the case of PBF LOC-3 test, the error in rupture time calculation was reduced in case of the extended model.

TABLE 6. EFFECT OF BALLOONING MODEL EXTENSIONS ON CALCULATED RUPTURE TIME

Test	Measured Rupture Temperature (K)	Measured Heating Rate at Rupture (K/s)	Rupture Time (s)		
				Calculated	
			Measured	Without Extensions	With Extensions
PBF LOC-3	1057	21	10.13	12.16	10.42
KfK	1076	3	70	62.7	62.7
Phebus	1326.4	56.25	12.76	10.93	10.93
TREAT FRF-2	1462	42.86	31.9	32.43	32.43

For the other cases, the model extensions had no effect on the rupture time. Since the cladding temperatures were input for the KfK test, an azimuthal variation in temperature would not be calculated and thus the model extensions would not have an effect on the calculated time of rupture. But for the Phebus and TREAT tests, the cladding azimuthal variation was calculated yet the model extensions had no effect on the calculated time of rupture. The absence of an effect for these two tests is considered to be due to the fact that the cladding ruptured while in the beta phase (temperature greater than 1250 K). Cladding rupture is not as sensitive to temperature variation in this phase as it is in the alpha to beta transition phase, which was the case for the PBF LOC-3 test.

4.2 Effect of Model Extensions on Transient Cladding Ballooning

Transient cladding ballooning cannot be directly measured. Instead, the transient ballooning is inferred from measurements of fuel rod internal pressure. The reciprocal relationship of gas volume to internal pressure is used to estimate transient cladding ballooning.

The measured internal pressure as a function of time is compared with the calculated pressures for the four tests in the Figures 21 to 24. In the case of PBF LOC-3 test, the comparison shows that the calculated values with the model extensions improved the agreement with the experimental data. For the other tests, the model extensions had no effect on the internal pressure behavior.

4.3 Effect of Model Extensions on Cladding Temperature

The cladding temperature at the rupture node is shown for the four tests in the Figures 25 to 28. The results show that for the PBF LOC-3 the model extensions cause the cladding oxidation to occur earlier (point 0 in Figure 23). This earlier oxidation results in a temperature difference for a short period of time (~3 seconds) between the calculated temperatures with and without the model extensions. The temperatures before and after the oxidation period are nearly the same. For the other tests, there is no influence of the model extensions on the cladding temperature.

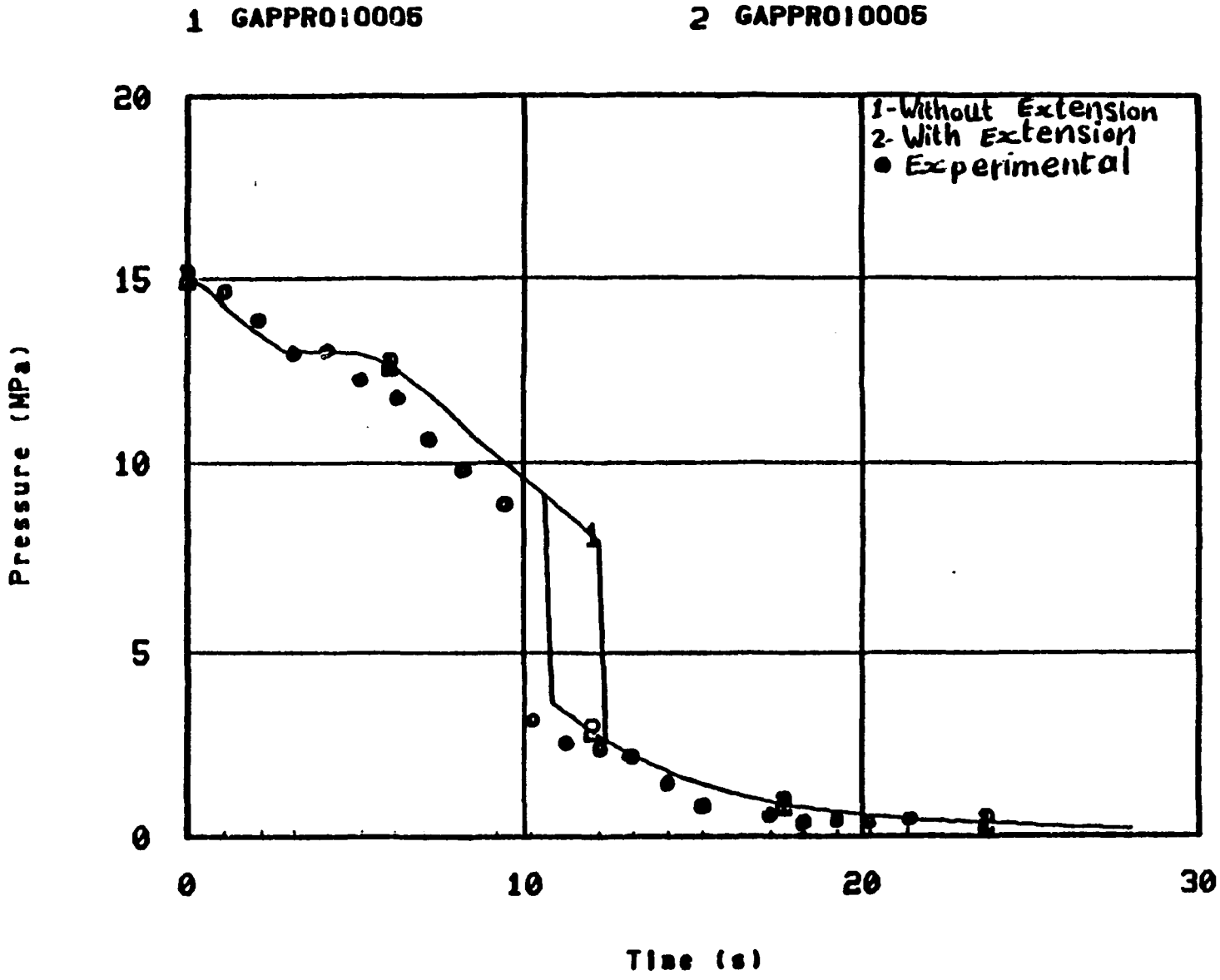

Figure 21. Variation of rod internal pressure as a function of time for PBF-LOC3

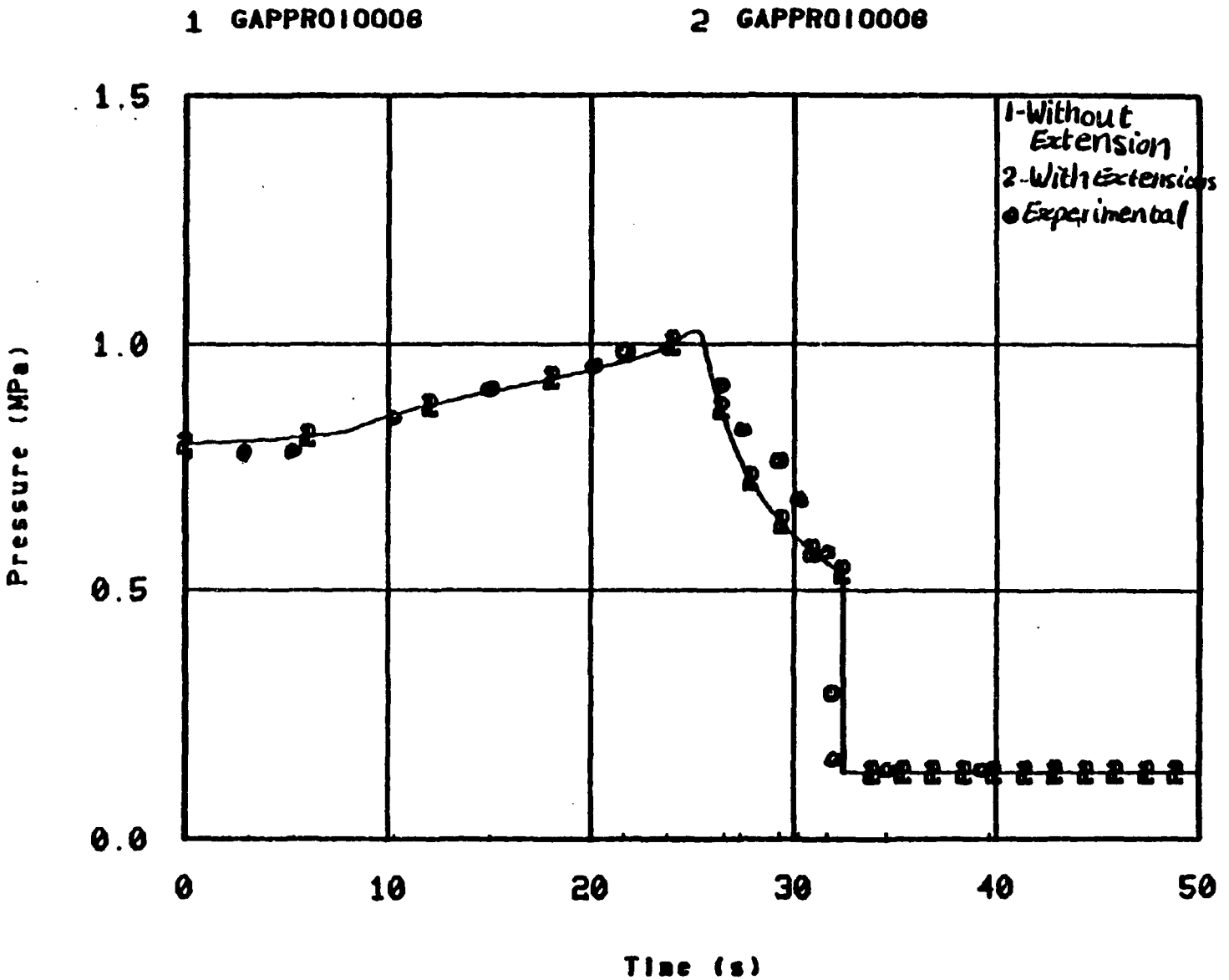

Figure 22. Variation of rod internal pressure as a function of time for TREAT

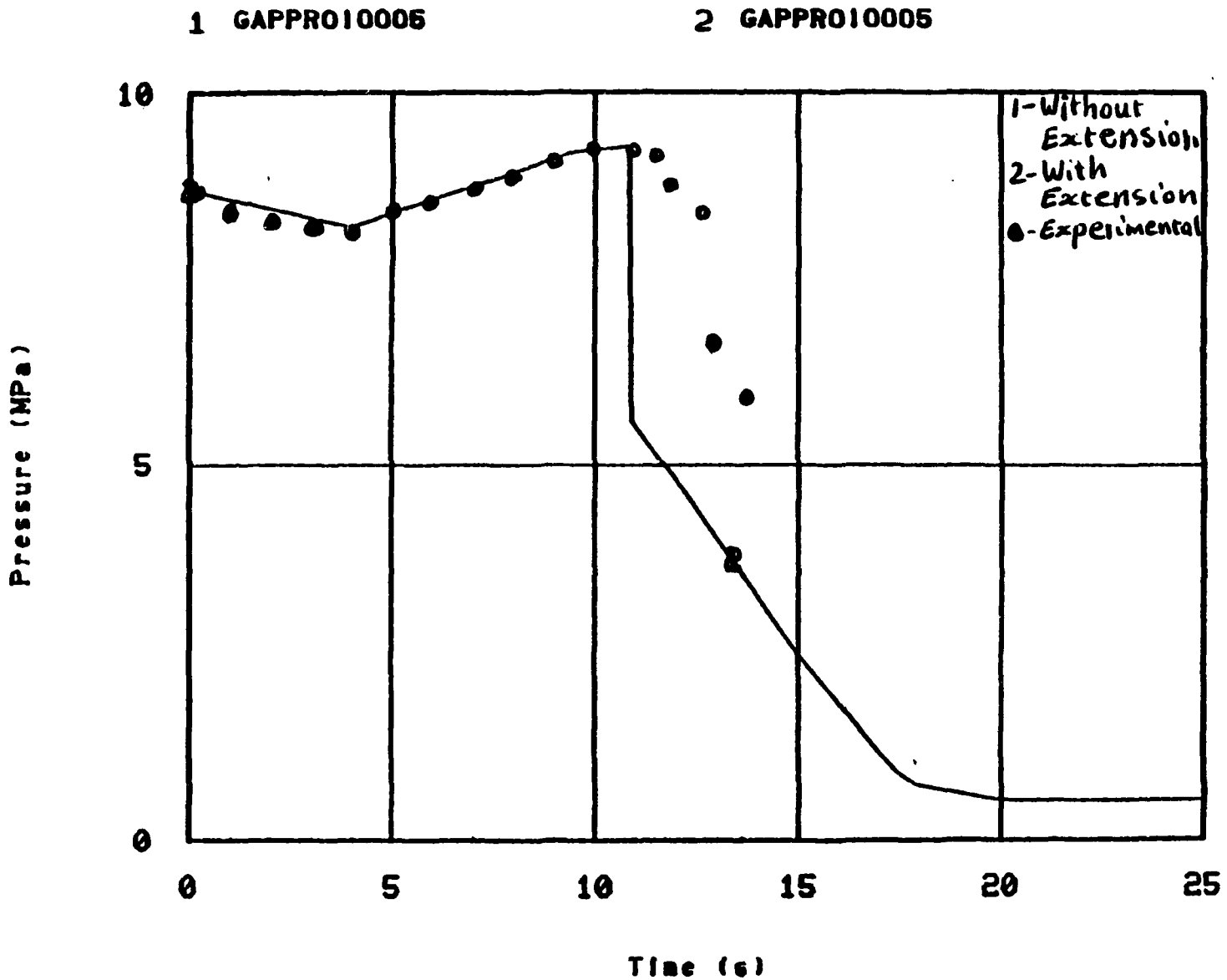

Figure 23. Variation of rod internal pressure as a function of time for Phebus

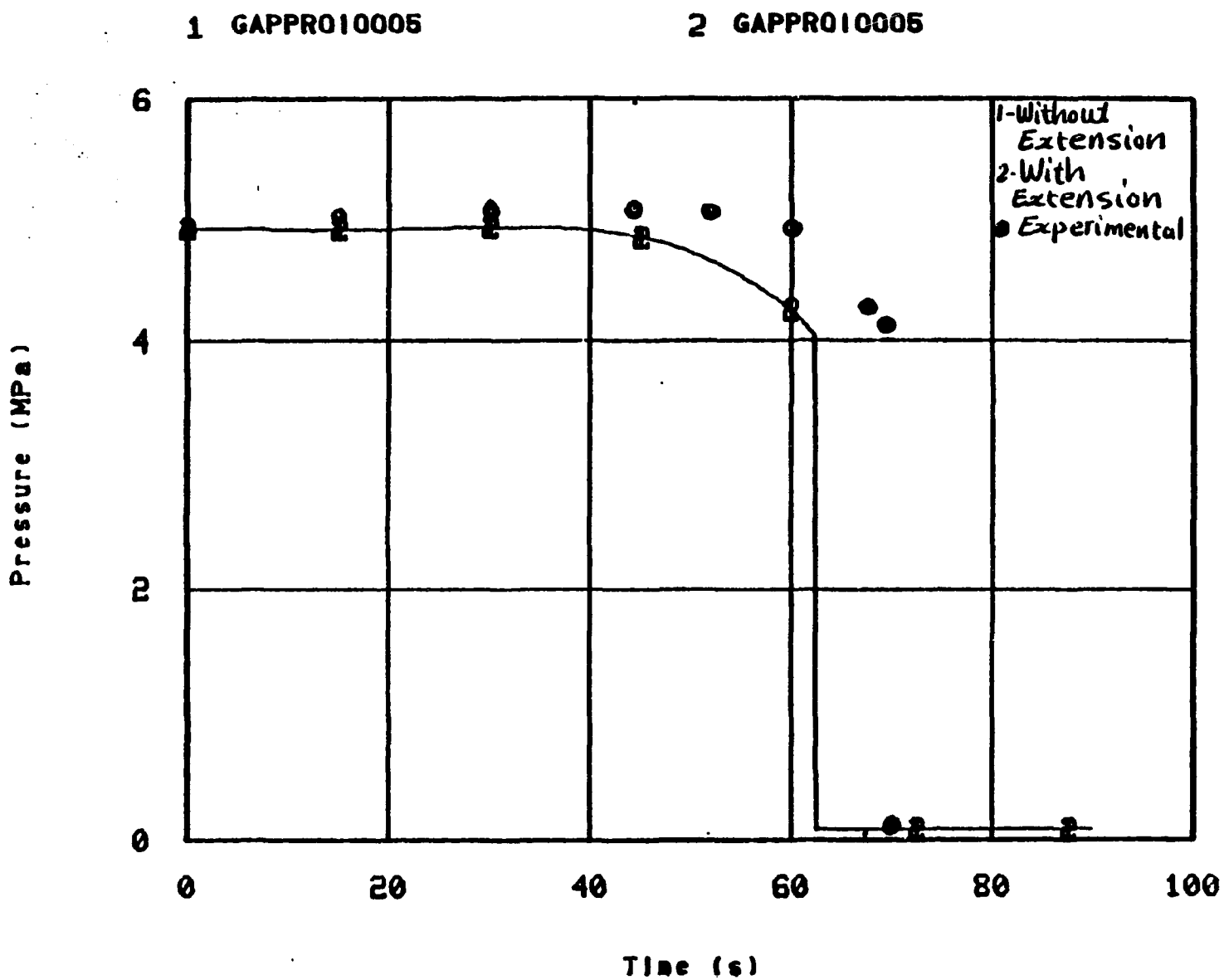

Figure 24. Variation of rod internal pressure as a function of time for KfK

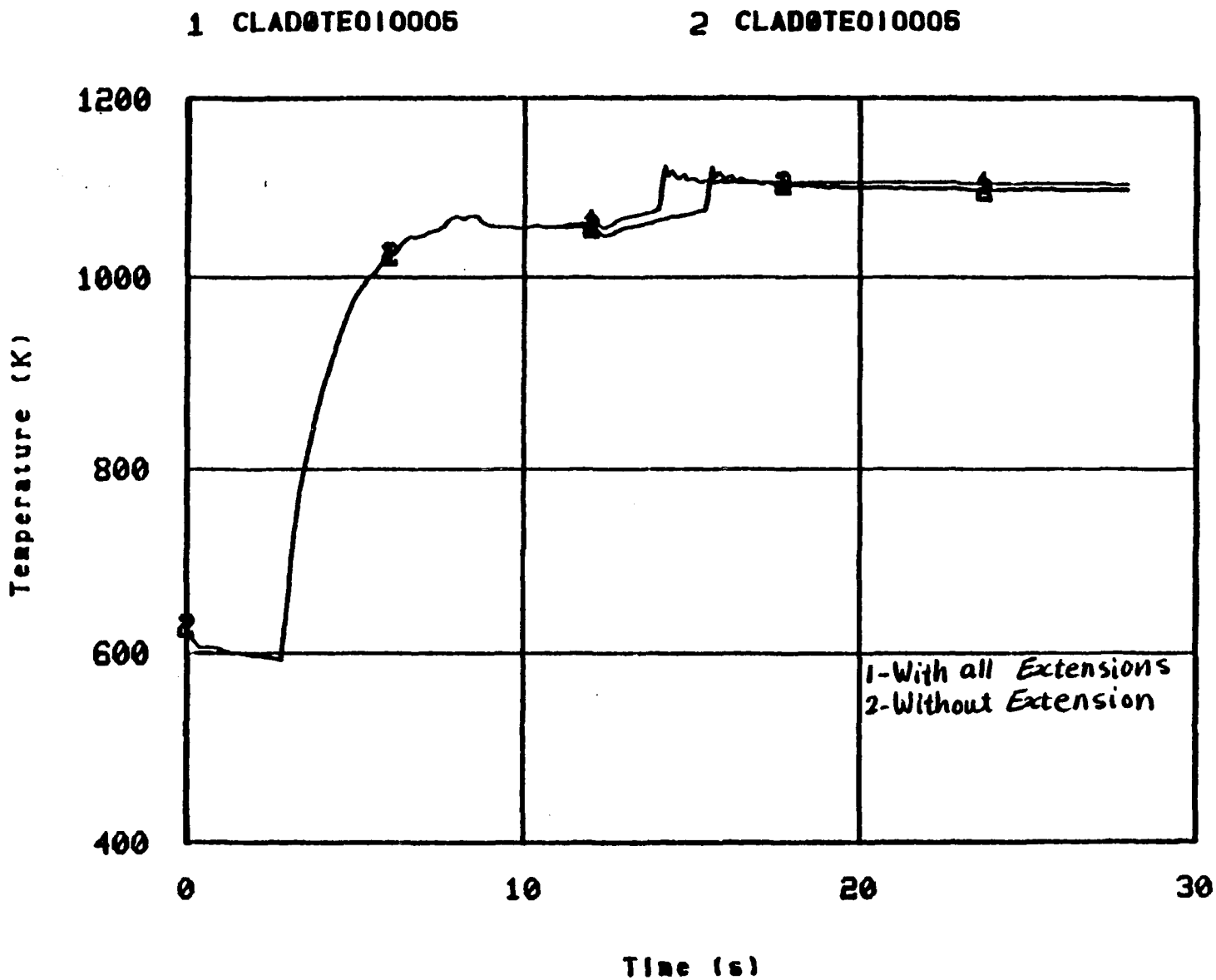

Figure 25. Cladding temperature as a function of time for PBF-LOC3

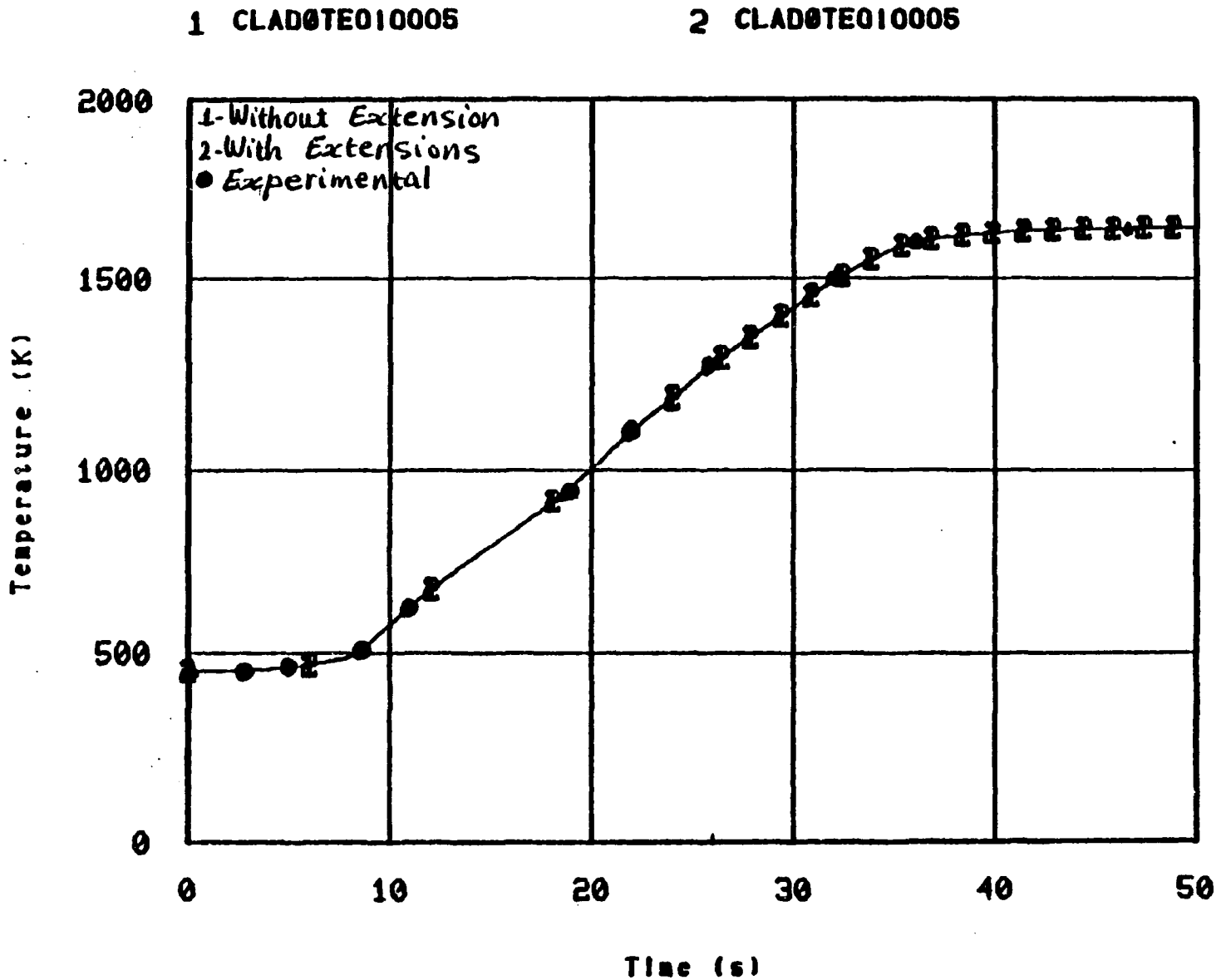

Figure 26. Cladding temperature as a function of time for TREAT

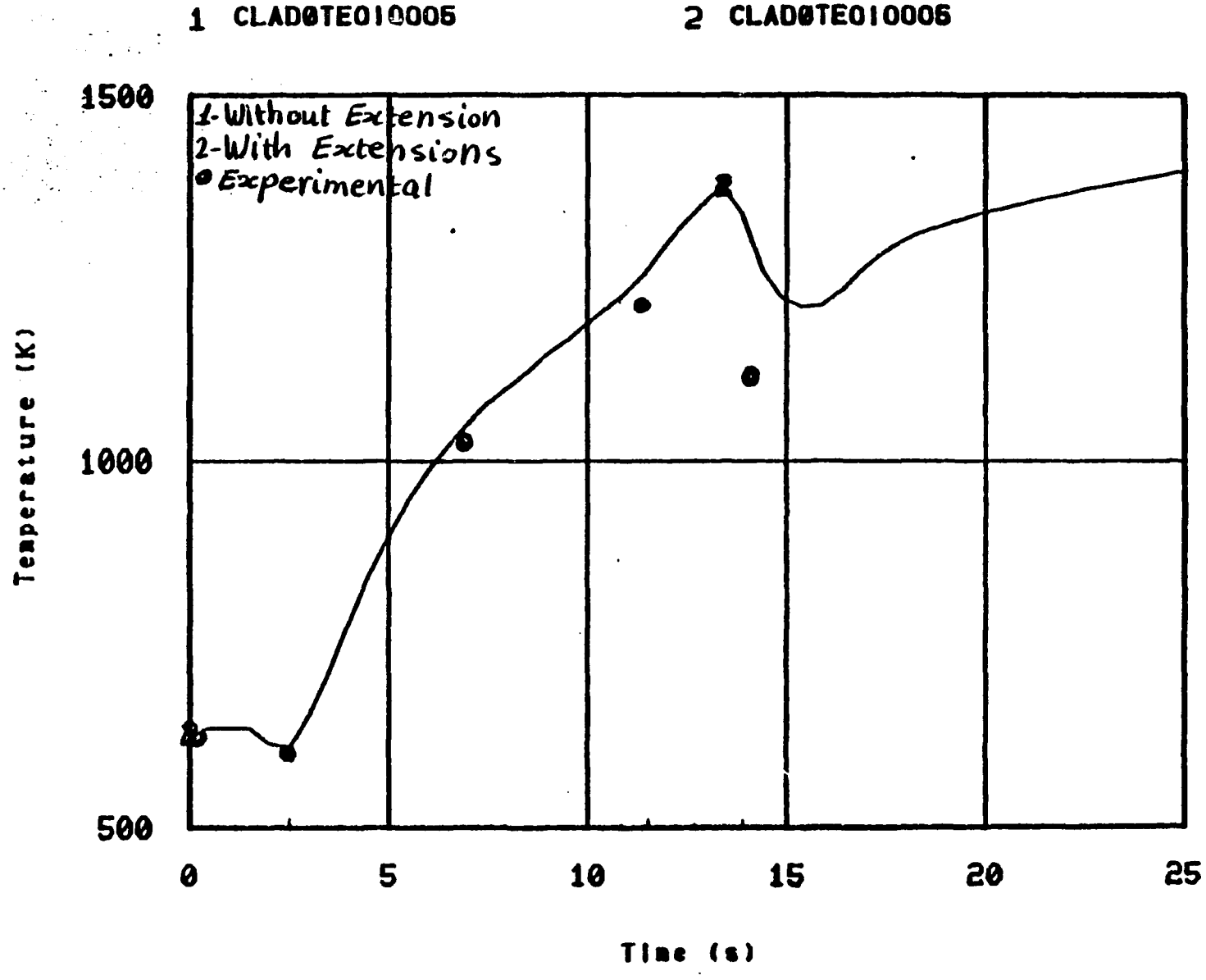

Figure 27. Cladding temperature as a function of time for Phebus

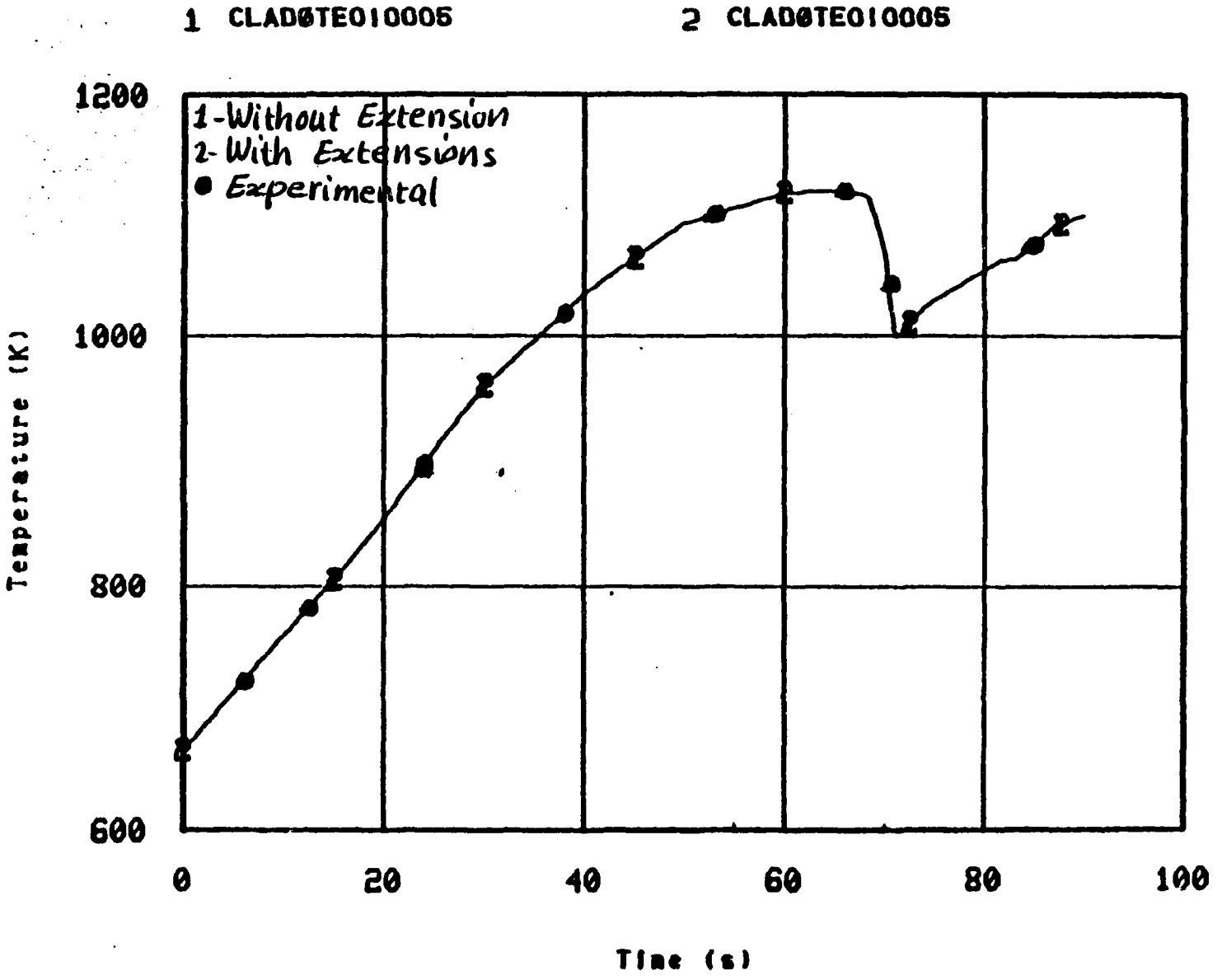

Figure 28. Cladding temperature as a function of time for KfK

4.4 Effect of Model Extensions on Permanent Hoop Strain

The measured hoop strain with and without the model extensions are compared with the experimental data in Figures 29 to 32. For the PBF-LOC-3 test (Figure 29), the calculated values are underestimated at the rupture location. The figure illustrates alsc that the location of rupture calculated by the code is higher than the actual rupture location. The calculated rupture location without the model extensions coincides with that calculated with the model extensions, but the calculated hoop strains without the model extensions are greater than those calculated with the model extensions. For both cases, the calculated and measured deformation profiles are in good agreement except for being offset about 0.05 m in elevation. As to the TREAT test (Figure 30), the calculated values with and without model extensions are nearly the same. In both cases, the calculated deformation is in good agreement with the measured deformation except for the calculated rupture location being about 0.05 m higher than the actual location. For the Phebus test (Figure 31), there is no difference between the values calculated with and without the model extensions. The measured rupture hoop strain varied between 4% and 35% and the measured rupture elevation varied from 0.2 and 0.4 m, and it is evident that the calculated values are within these ranges. The cause for the wide variation in experimental results is not known. In the KfK test (Figure 32), both the values calculated with and without the model extensions are coincident. The calculated rupture strain is about half of the measured value but the calculated rupture location is in good agreement with the measured location.

Both the calculations and the experimental results show that coplanar blockage does not occur during conditions typical of a large break LOCA. Blockage does not occur unless cladding hoop strains exceed 65% over several cm of length. None of the experimental results show that blockage occurred. The cladding hoop strain was calculated to exceed 65% only for the TREAT FRF-2 experiment. But even for this case, the calculated hoop strain exceeded 65% over a span of elevation so small that coplanar blockage could not occur.

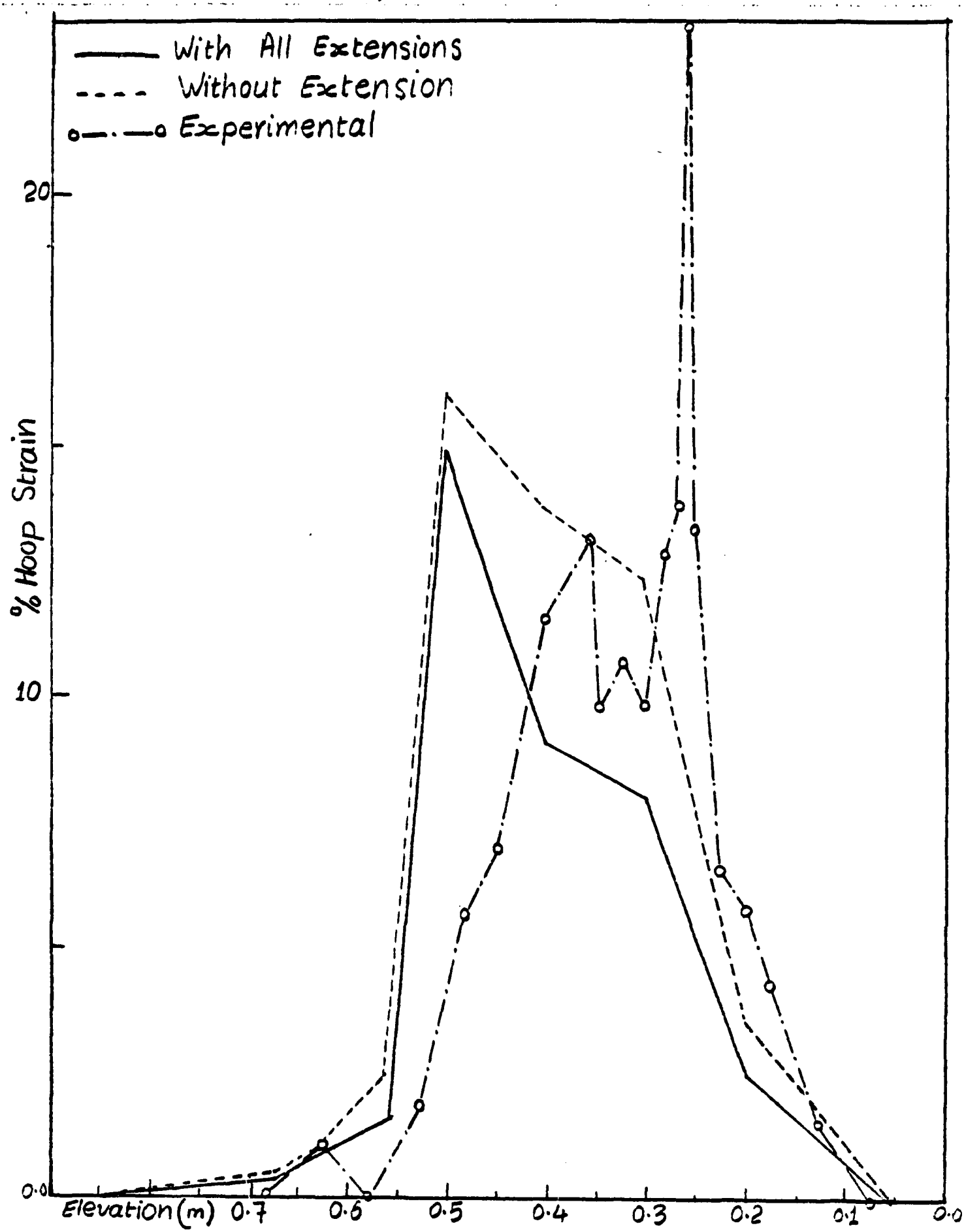

Figure 29. Axial hoop strain distribution for PBF-LOC3

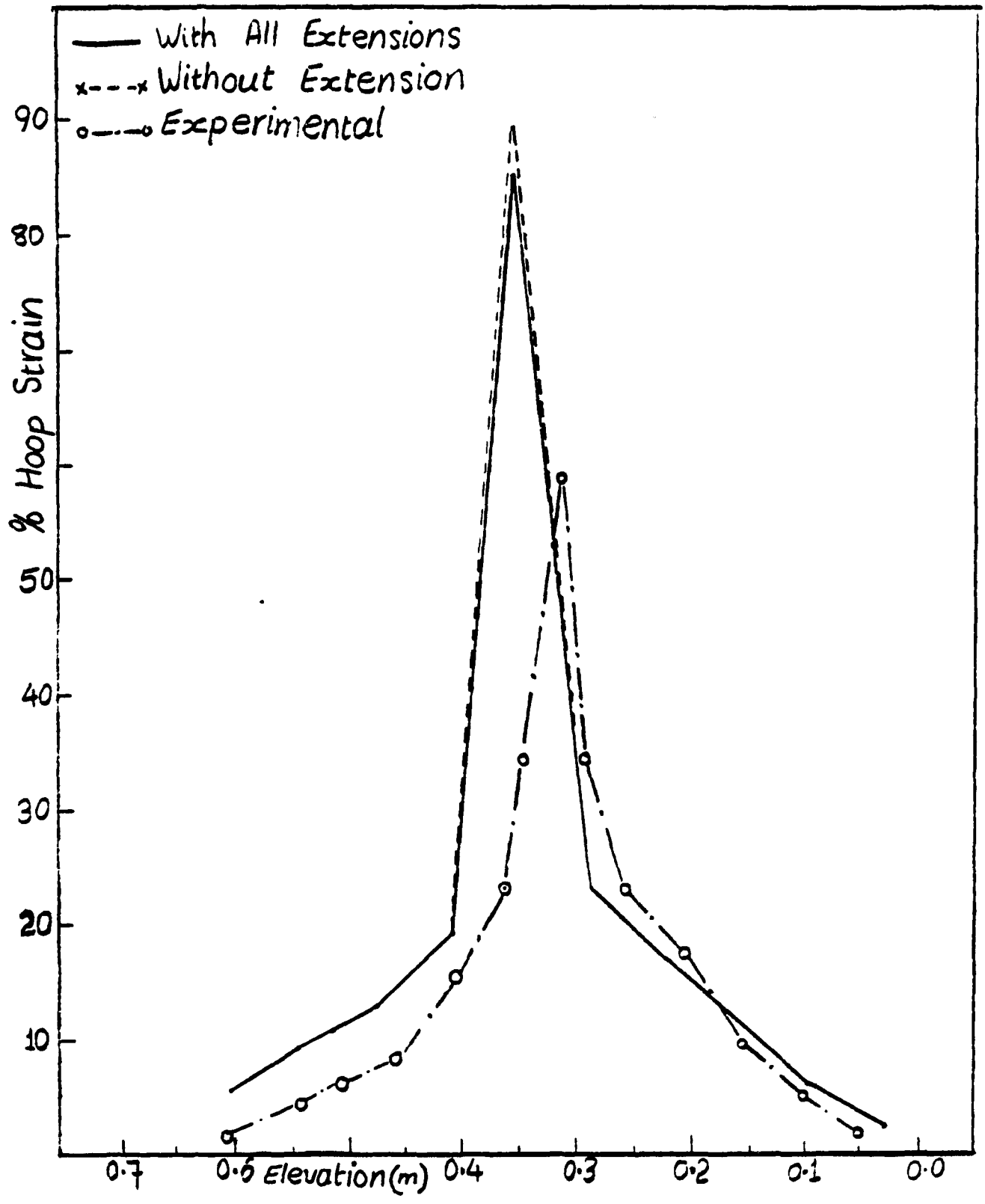

Figure 30. Axial hoop strain distribution for TREAT

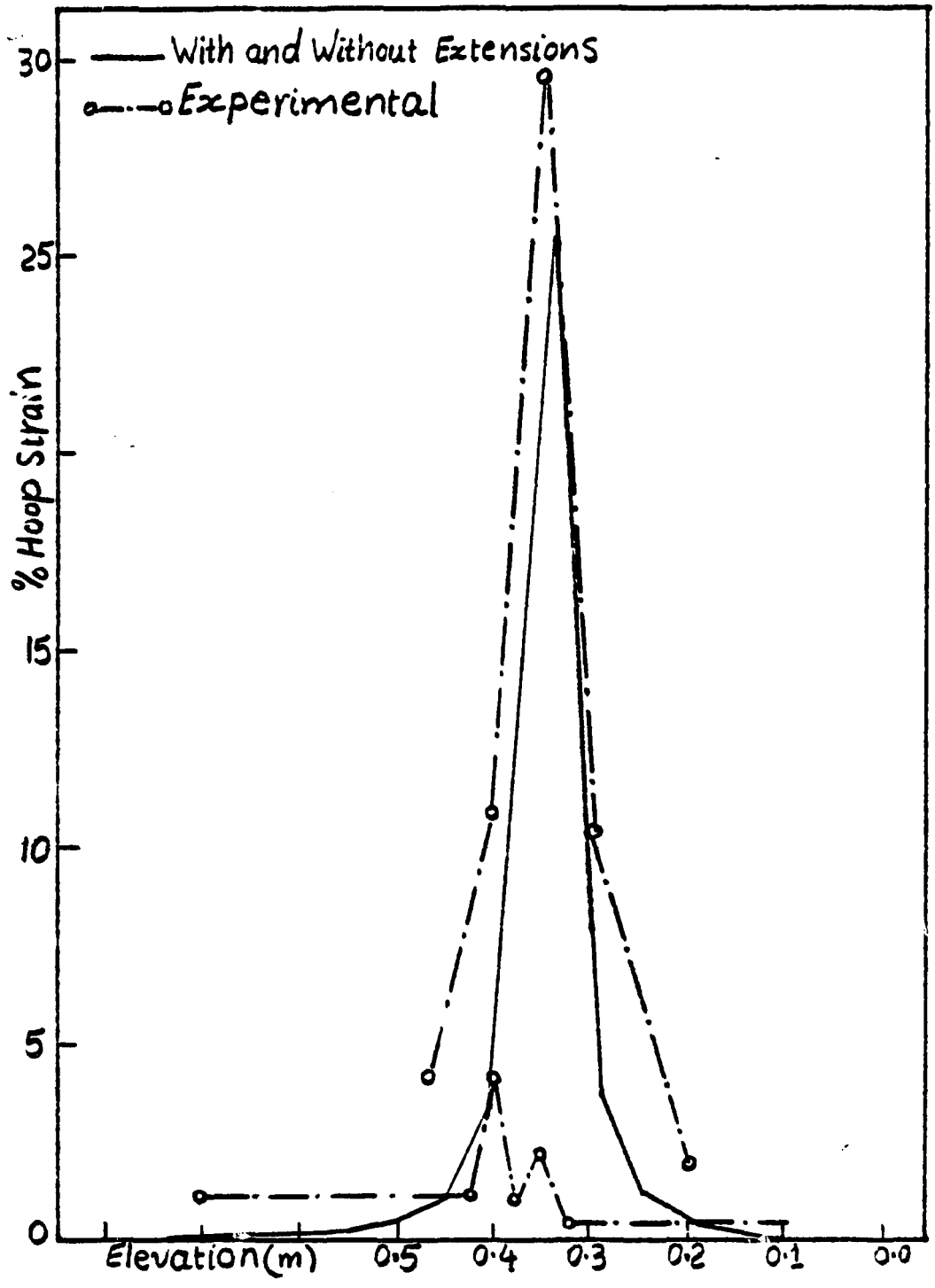

Figure 31. Axial hoop strain distribution for Phebus

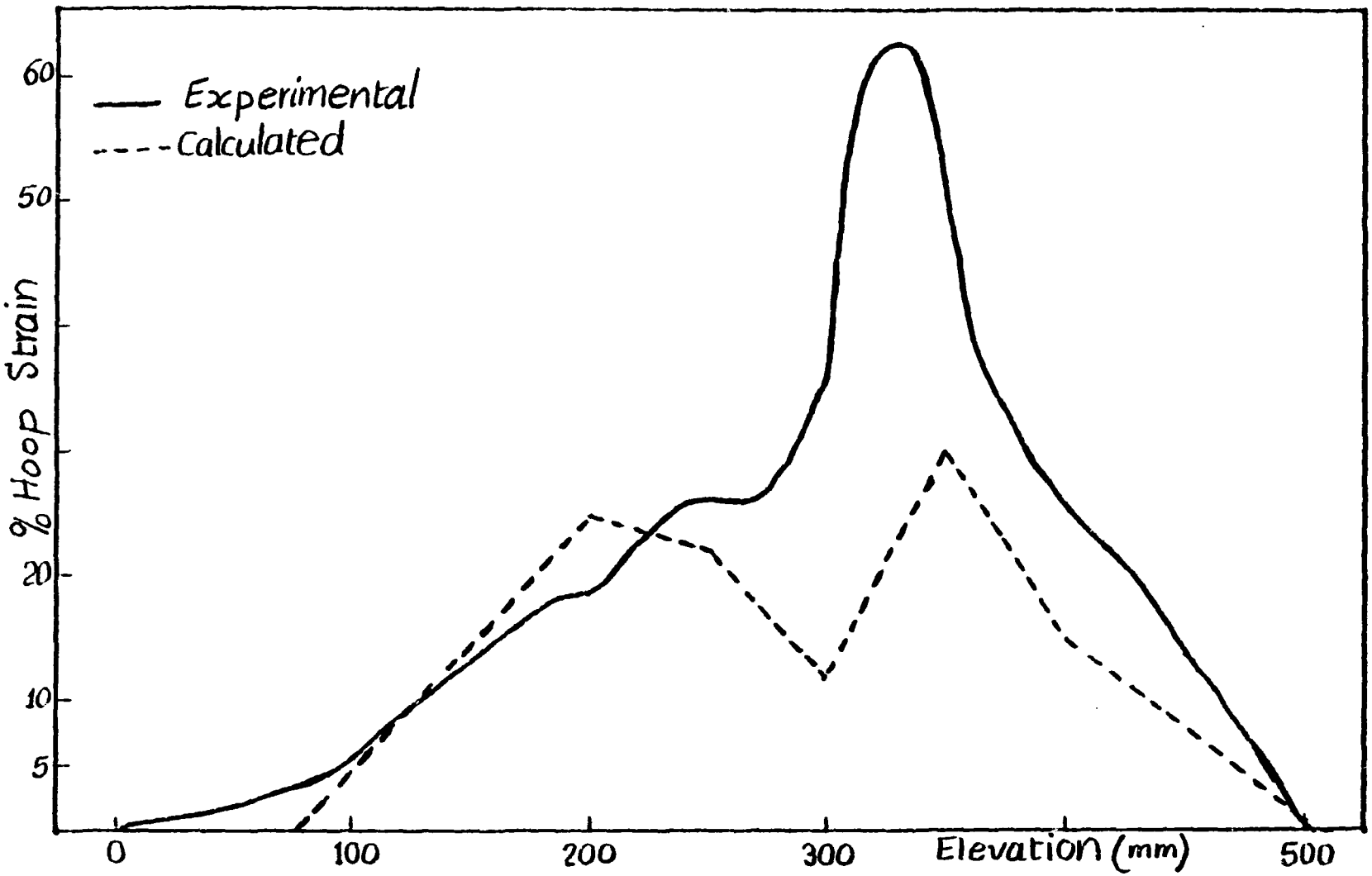

Figure 32. Axial hoop strain distribution for KfK

5. IN-DEPTH STUDY OF MODEL EXTENSIONS

In order to investigate the effect of the various parts of the extensions to the ballooning model, the fuel rod experiments were calculated by FRAP-T6 with only parts of the model extension employed. The work done term and azimuthal heat conduction were studied using the PBF LOC-3 test. The effect of all these parameters on the internal pressure is shown in Figure 33 and the effect on the rupture time is shown in Table 7.

Comparisons of the calculated rupture times presented in Table 7 reveal that the work done term had no effect on the calculated rupture time and that the modeling of cladding azimuthal heat conduction had only a minor effect. The major effect on the calculated rupture time was the model extension that calculated the temperature distribution on the surface of fuel pellets.

The effect on the cladding temperature at Node 5 is shown in Figure 34. From the internal pressure and the cladding temperature it can be said that the work done term has no influence and the cladding azimuthal heat conduction contribution is small.

The following analysis shows why the work done term and the modeling of cladding azimuthal heat conduction did not influence the calculated time of rupture.

The work done is equal to:

2π[(circumferential stress)(circumferential strain rate)(average radius)(initial thickness)][exp(radial strain)]

For the PBF LOC-3 test at the rupture location at a time, just before rupture,

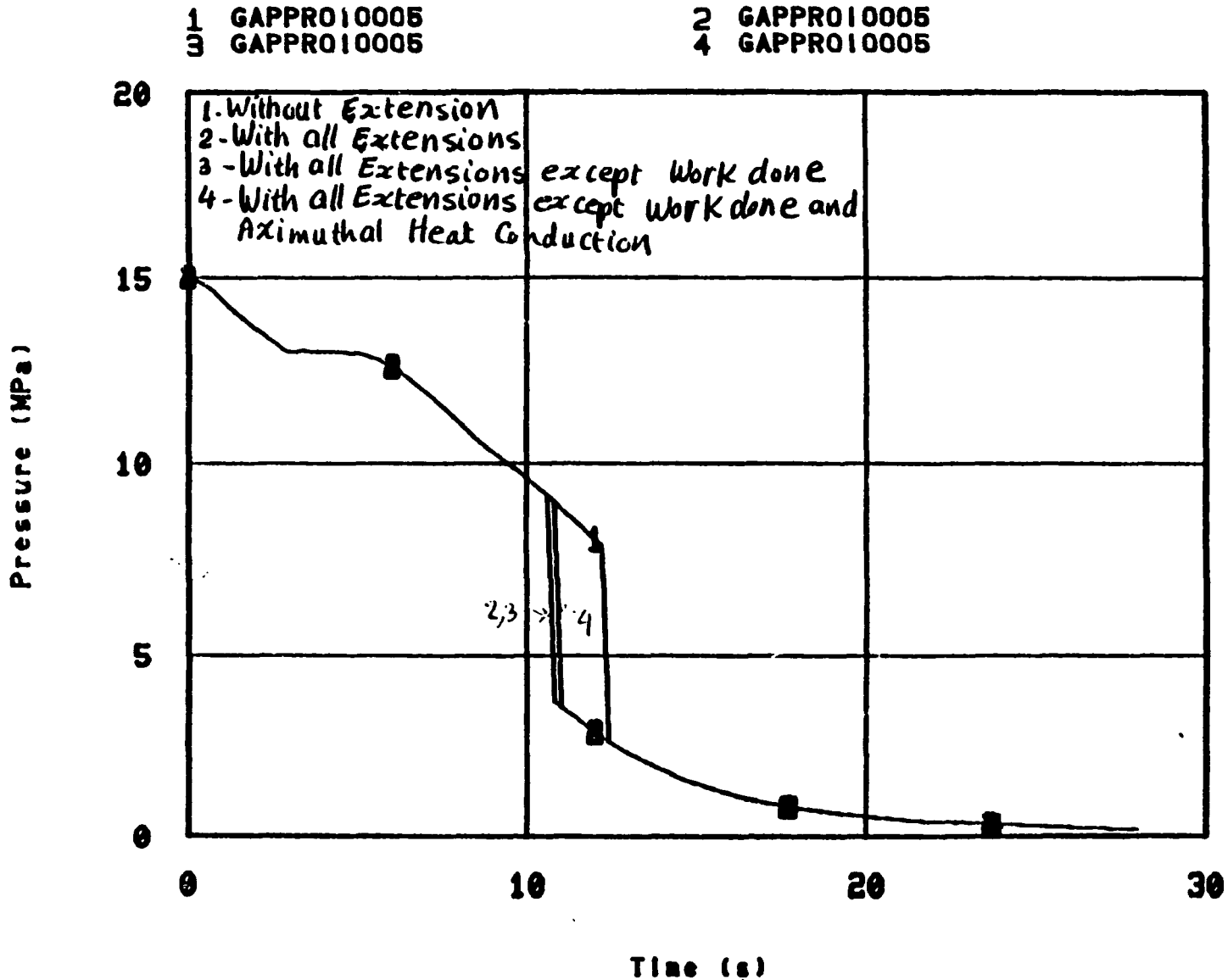

Figure 33. Variation of rod internal pressure as a function of time for PBF-LOC3

TABLE 7. EFFECT OF WORK DONE TERM AND AZIMUTHAL HEAT CONDUCTION ON THE RUPTURE TIME

Case	Rupture Time (s)
Measured	10.13
Without any model extensions	12.16
All model extensions except work done and azimuthal heat conduction in the cladding	10.86
All model extensions except work done	10.42
All model extensions	10.42

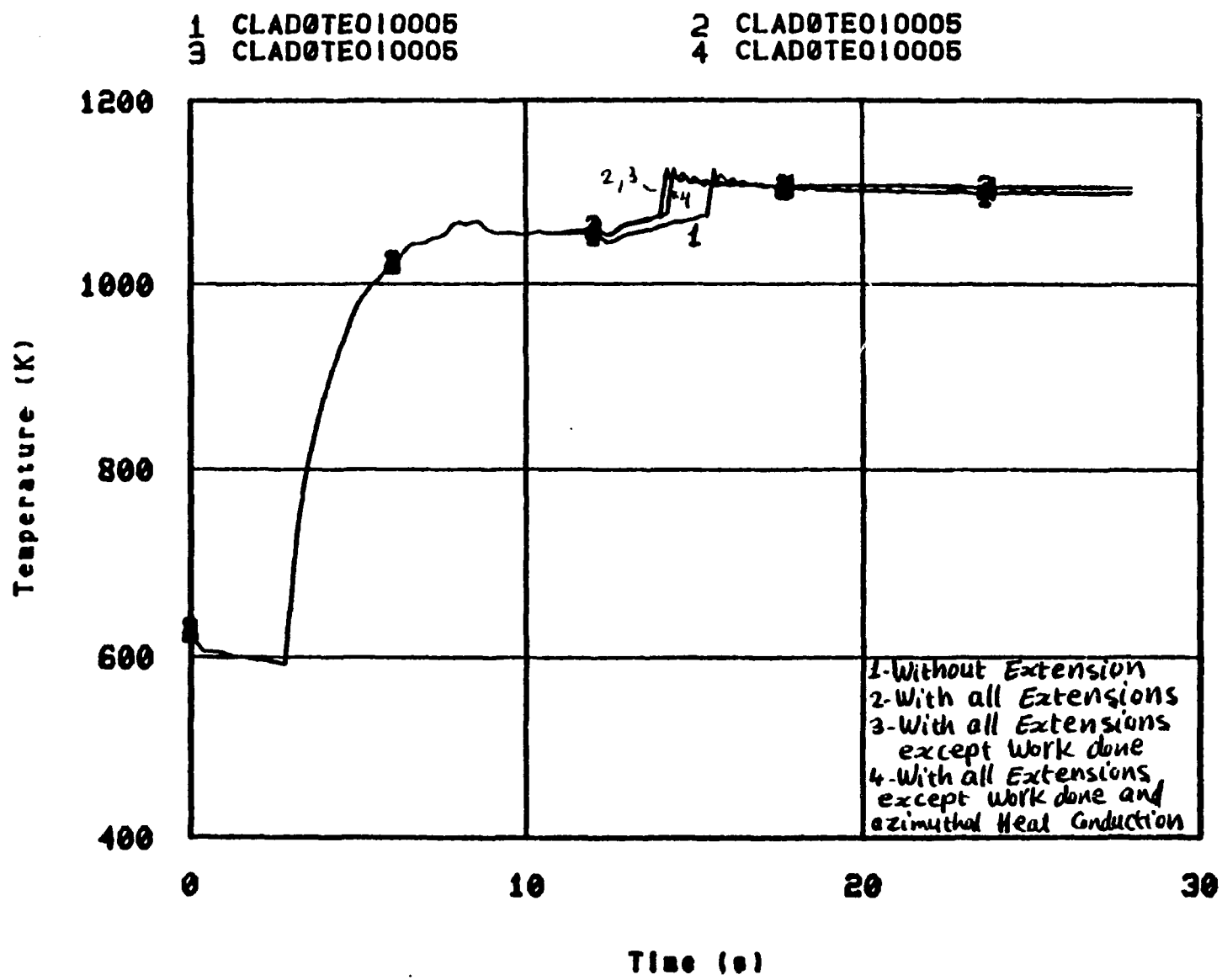

Figure 34. Cladding temperature as a function of time for PBF-LOC3

Stress = 4×10^7 N/m^2,

Strain rate = 0.023 per s,

Strain = 0.1037

Wall thickness = 0.53×10^{-3} m

Average radius = 0.52×10^{-2} m

Work done = $(2\pi)[4\ 10^7(2.3 \times 10^{-2})(5.3 \times 10^{-4})$
$(5.2 \times 10^{-3})[\exp(0.1037)]$

= 18.26 W/m

The azimuthal heat conduction at the Node J is equal to:

$$E_j = \frac{(T_{j-1} - T_j)}{0.5(r_j - 1 + r_j)\ \Delta\ \theta}\ [0.5(h_{j-1} + h_j)]\ 0.5(K_{j-1} + K_j)$$

$$+ \frac{(T_j - T_{j+1})}{\Delta\ \theta\ 0.5(r_j + r_{j+1})}\ [0.5(h_j + h_{j+1})]\ 0.5(K_j + K_{j+1})$$

where

T = cladding temperature (k)

r = cladding radius (m)

h = cladding thickness (m)

k = cladding thermal conductivity (W/m - k)

E_j = heat transferred into element j by azimuthal heat conduction (W/m)

For Nodes 7, 8, 9;

$T_7 = 1133$ $T_8 = 1110$ $T_9 = 1099$

$r_7 = 4.9836 \times 10^{-3}$ $r_8 = 5.3053 \times 10^{-3}$ $r_g = 5.6478 \times 10^{-3}$ m

$h_7 = 5.43798 \times 10^{-4}$ $h_8 = 5.48642 \times 10^{-4}$ $h_g = 5.525 \times 10^{-4}$ m

$K = 22$ W/m • k

$E_8 = 398$ W/m.

The heat transferred from the fuel, E_f is given by the equation

$E_f = 2 \pi \times T_f \times h_{gap} \times$ (fuel radius)

$T_f = 1130$ K; hgap (gap heat transfer coefficient) $= 1.47 \times 10^3$.

Thus,

$E_f = 2 \pi \times 1130 \times 1.67 \times 10^3 \times 4.935 \times 10^{-3}$

$= 0.350526 \times 10^5$ W/m .

The azimuthal temperature variation for the fuel and cladding are shown in Figures 35 to 39.

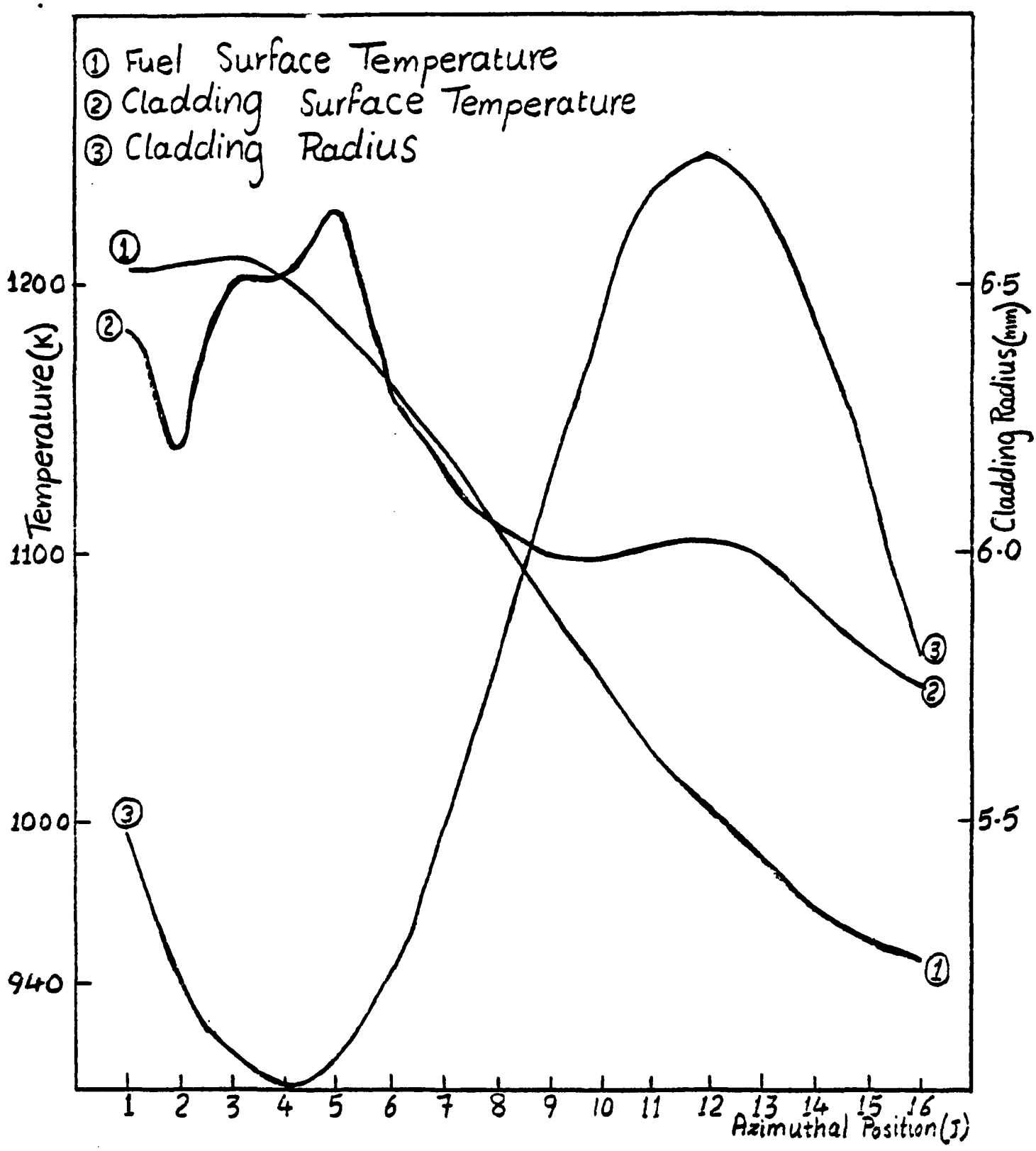

Figure 35. Azimuthal variation of fuel surface temperature, cladding surface temperature and cladding radius for PBF-LOC3

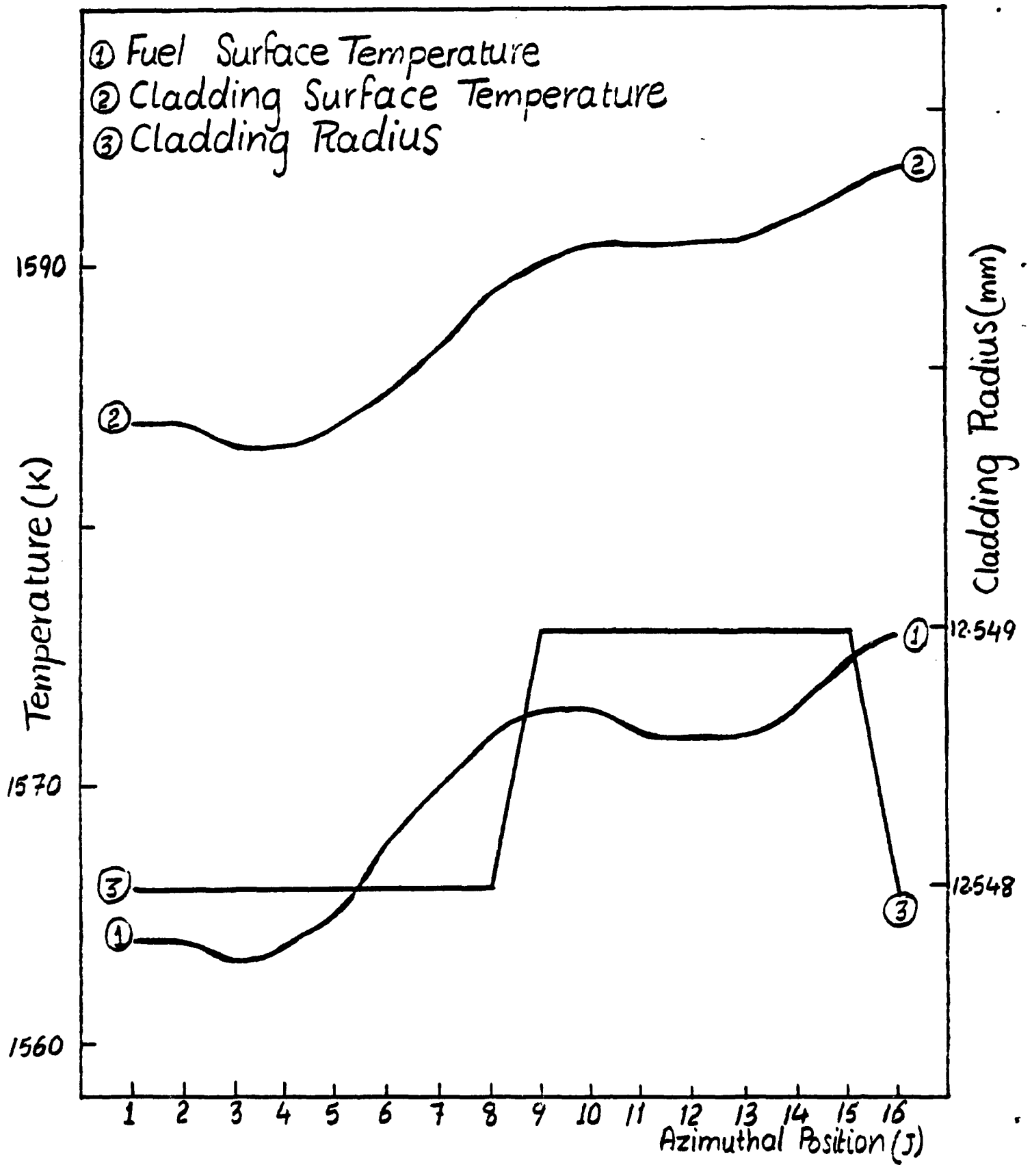

Figure 36. Azimuthal variation of fuel surface temperature, cladding surface temperature and cladding radius for TREAT

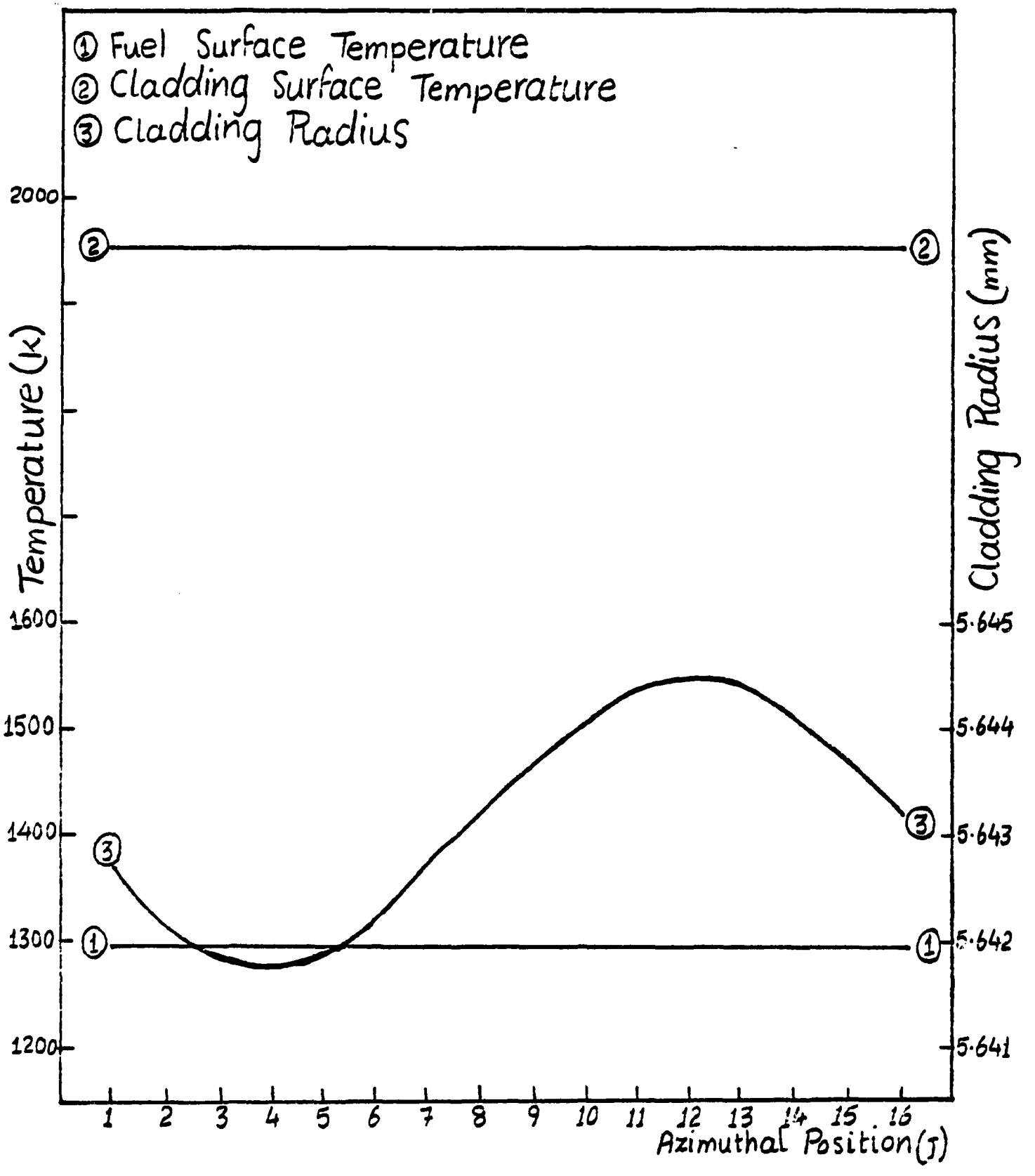

Figure 37. Azimuthal variation of fuel surface temperature, cladding surface temperature and cladding radius for Phebus

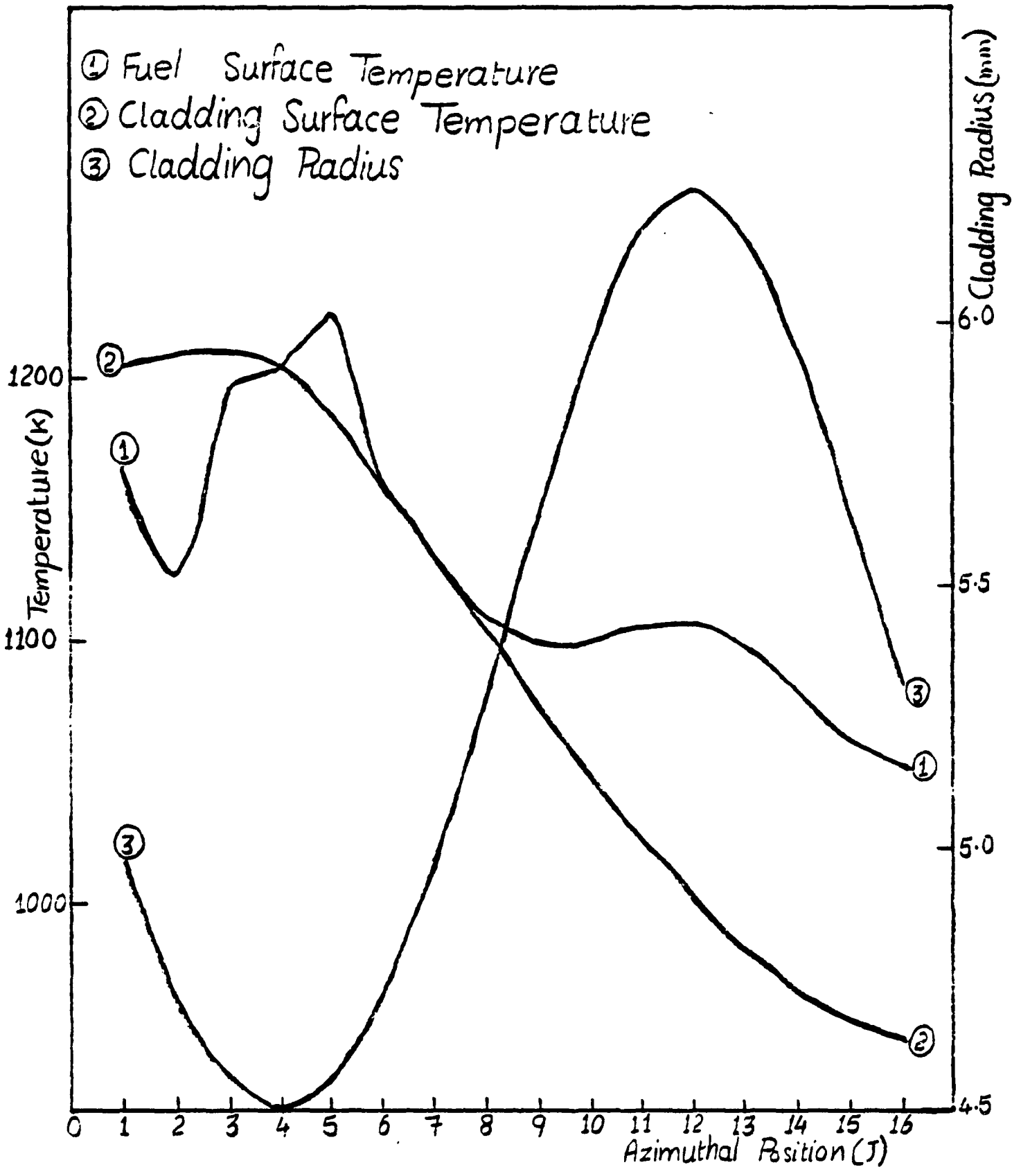

Figure 38. Azimuthal variation of fuel surface temperature, cladding surface temperature and cladding radius for PBF-LOC3 (case of all extensions except work done)

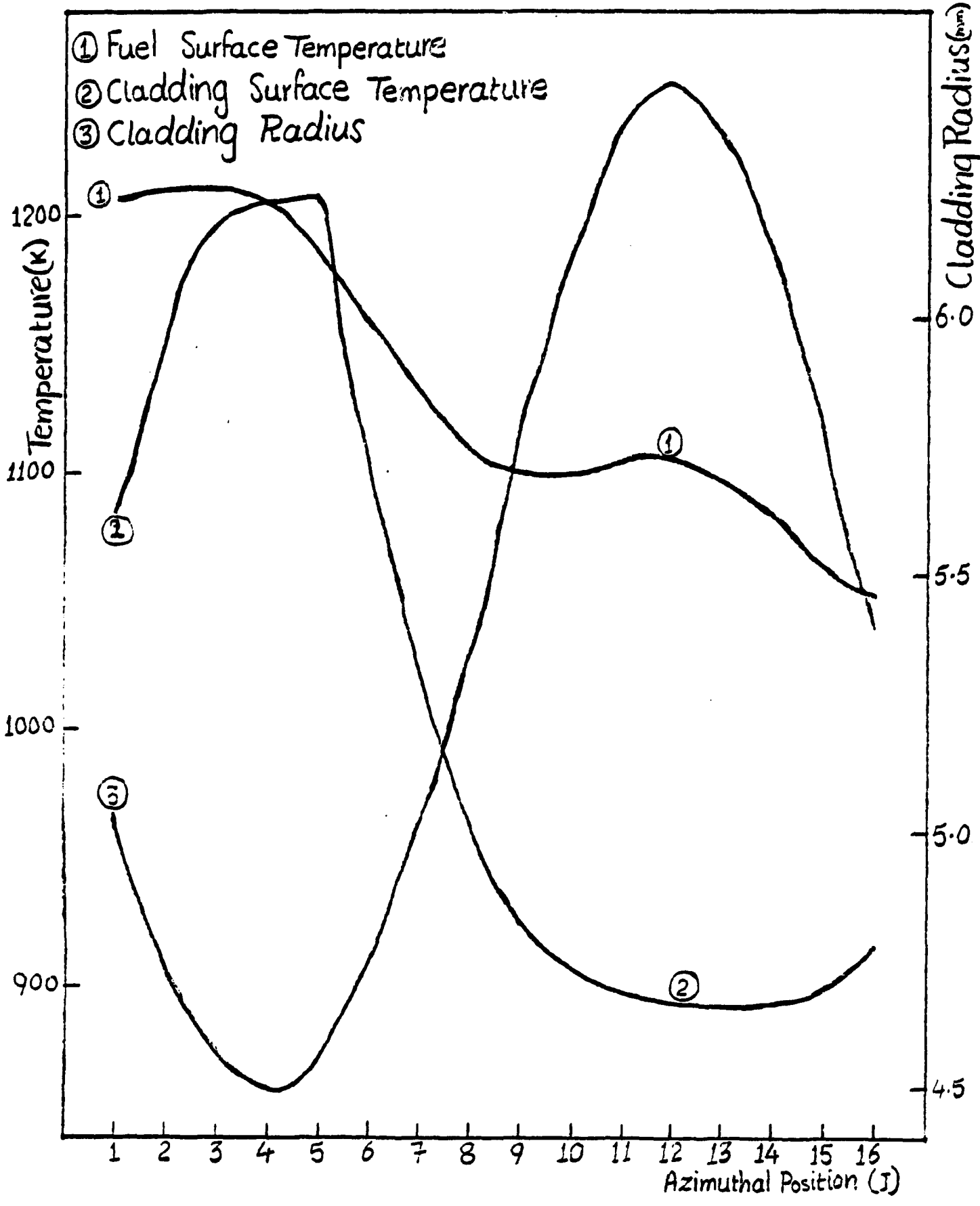

Figure 39. Azimuthal variation of the fuel temperature, cladding surface temperature and cladding radius for PBF-LOC3 (case of all extensions except work done and azimuthal heat conduction)

6. CONCLUSIONS

The FRAP-T6 code was extended to calculate: (a) fuel surface azimuthal temperature distribution; (b) work done on cladding by internal pressure; and (c) azimuthal heat conduction in the cladding. The extensions were assessed by comparing calculated and measured cladding ballooning characteristics for four in-pile fuel rod tests. The assessment showed that the calculation of the fuel surface azimuthal temperature distribution improved the calculations of cladding ballooning during the alpha to beta phase transition. The modeling of the work done on cladding and azimuthal heat conduction in the cladding had an insignificant effect on the calculation of cladding ballooning for beta phase cladding and LOCA conditions. The assessment also showed that FRAP-T6 calculations of cladding ballooning using the BALON2 model are in good agreement with experimental results. Both calculations and experimental results indicate that coplanar blockage due to cladding ballooning is unlikely during a large break LOCA.

7. REFERENCES

1. Code of Federal Regulations, 10 CFR 50, Appendix K, U.S. Government Printing Office, 1986.

2. J. M. Broughton and P. E. MacDonald, Light Water Reactor Fuel Behavior Program Description: PBF-LOCA Experiment Requirements, TFBP-TR-201, January 1975.

3. R. H. Chapman, Multirod Burst Test Program Progress Report for July-December 1977, NUREG/CR-0103, ORNL/NUREG/TM-200, June 1978.

4. D. L. Hagrman, Zircaloy Cladding Shape at Failure (BALON2), EGG-CDAP-5379, July 1982.

5. L. J. Siefken et al., FRAP-T6: A Computer Code for the Transient Analysis of Oxide Fuel Rods, NUREG/CR-2148, EGG-2104, May 1981.

6. G. Sdouz, "BALO-A: An Extended Fuel Rod Deformation Code," Trans. American Nuclear Society, 47, p. 265, 1984.

7. D. L. Hagrman, private communications, November 1986.

8. R. Nijsing, "Temperature and Heat Flux Distribution in Nuclear Fuel Element Rods," Nuclear Engineering and Design, 4, pp. 1-20, 1966.

9. J. M. Broughton et al., PBF LOCA Test Series, Tests LOC-3 and LOC-5 Fuel Behavior Report, NUREG/CR-2073, EGG-2094, June 1981.

10. E. H. Karb et al., LWR Fuel Rod Behavior in the FR2 In-Pile Test Simulating the Heatup Phase of a LOCA Final Report, KfK-3346, March 1983.

11. E. S. DeMartinville and M. Pignard, Behavior of a Bundle During a Two-Peaks Large Break LOCA Temperature Transient Preliminary Comparison Report, CEA/CEN - CADARACHE, IPSN/DERS/SEAREL, 1985.

12. R. A. Lorenz and G. W. Parker, Final Report on the Second Fuel Rod Failure Transient Test of a Zircaloy-Clad Fuel Rod Cluster in TREAT, ORNL-4710, January 1972.

13. V. H. Ransom et al., RELAP5/MOD2 Code Manual, Volumes 1 and 2, NUREG/CR-4312, EGG-2396, August 1985.

FIGURE CAPTION LIST

END

DATE FILMED

04 / 06 / 88